frontiers | Frontiers in Earth Science

TYPE Original Research
PUBLISHED 10 October 2023
DOI 10.3389/feart.2023.1128798

OPEN ACCESS

EDITED BY
Basilios Tsikouras,
Universiti Brunei Darussalam, Brunei

REVIEWED BY
Karoly Nemeth,
Institute of Earth Physics and Space Sciences, Hungary
Jorge Eduardo Romero,
Universidad de O'Higgins, Chile
Dmytro Hlavatskyi,
National Academy of Sciences of Ukraine, Ukraine

*CORRESPONDENCE
Aditya Pratama,
aditya.pratama@brin.go.id
Mirzam Abdurrachman,
mirzam@gl.itb.ac.id

RECEIVED 21 December 2022
ACCEPTED 22 September 2023
PUBLISHED 10 October 2023

CITATION
Pratama A, Nurfiani D, Suryanata PB, Ismail T, Bunga Naen GNR, Abdurrachman M, Supriyadi Banggur WF, Asri NS, Nareswari RB, Bijaksana S, Hanif M, Kriswati E, Kurniawan IA and Setiawan NI (2023), Magma storage conditions beneath Krakatau, Indonesia: insight from geochemistry and rock magnetism studies.
Front. Earth Sci. 11:1128798.
doi: 10.3389/feart.2023.1128798

Magma storage conditions beneath Krakatau, Indonesia: insight from geochemistry and rock magnetism studies

Aditya Pratama[1,2]*, Dini Nurfiani[2], Putu Billy Suryanata[2,3], Taufik Ismail[1,2,4], Gabriela Nogo Retnaningtyas Bunga Naen[2], Mirzam Abdurrachman[1,4]*, Wilfridus Ferdinando Supriyadi Banggur[2], Nining Sumawati Asri[5], Ratika Benita Nareswari[2], Satria Bijaksana[3], Muhammad Hanif[2], Estu Kriswati[2], Idham Andri Kurniawan[1,4] and Nugroho Imam Setiawan[6]

[1]Faculty of Earth Sciences and Technology, Bandung Institute of Technology, Bandung, Indonesia, [2]Research Center for Geological Disaster, National Research and Innovation Agency (BRIN), Bandung, Indonesia, [3]Faculty of Mining and Petroleum Engineering, Bandung Institute of Technology, Bandung, Indonesia, [4]Department of Geological Engineering, Sekolah Tinggi Teknologi Mineral Indonesia, Bandung, Indonesia, [5]Research Center for Advanced Materials, National Research and Innovation Agency (BRIN), Tangerang Selatan, Indonesia, [6]Geological Engineering Department, Engineering Faculty, Universitas Gadjah Mada, Yogyakarta, Indonesia

Understanding the evolution of magma storage conditions on volcanoes which have had more than one caldera-forming eruption (CFE) is important to know about past and present conditions, as a key to forecast future potential hazards. Krakatau volcano is characterized by cyclic phases of growth and destruction of the edifice. A volcanostratigraphic study identified three eruptive periods: Old Krakatau, Young Krakatau, and Anak Krakatau. The Old and Young Krakatau periods ended with the first and second CFE respectively. Due to its permanent activity and edifice evolution, Krakatau poses a high risk on the surrounding inhabited islands. In this study, we combined geochemistry, rock magnetic, and petrology to infer the evolution of magma storage conditions from Old to Anak Krakatau periods. This study is the first to report on the chemical and rock magnetic characteristics, as well as storage system conditions of Old Krakatau and its relation to the ongoing evolution of Krakatau. Our data show that: 1) Old and Young Krakatau magma storage regions are shallow (within the upper 3 km), contain more differentiated magmas, from which the Old Krakatau magmas may be less oxidized and had lower temperatures than Young Krakatau; 2) Anak Krakatau magma storage is deeper (up to 26 km), less differentiated, and erupted hotter but more reduced compared to Old and Young Krakatau. The Old and Young Krakatau lavas were the products of pre-CFE and their chemical characteristics are included at maturation phase, whereas the Young Krakatau pumice samples were the product of the second CFE. Lastly, the post-second CFE activity of AK is currently in an incubation phase and represented by mafic products of frequent and small eruptions. Knowing that the volcano has experienced maturation and CFE phases in the past, the current AK may evolve to those phases in the future.

KEYWORDS

Krakatau, petrology, rock magnetism, magnetic minerals, mineral chemistry, magma storage

1 Introduction

Krakatau volcano is a globally well-known volcano due to its eruptive history and active volcanism. There have been at least two reported caldera-forming eruptions (CFE), with at least one impacting nearby inhabited island (Supplementary Figure S1). Far before the famous 1883 explosive eruption, the volcano experienced a series of significant volcanic events involving eruption, growth, and collapse of the volcanic edifice. The collapse events correspond to the CFE that occurred presumably in AD 416 and in 1883 (Stehn, 1929; Bronto, 2000; Winchester, 2003). It shows an evolution of the CFEs (i.e., caldera cycle) similar to that of other calderas: Campi Flegrei, Kos-Nisyros Volcanic Complex, Long Valley, Rabaul, and Okataina (Forni et al., 2018; Bouvet de Maisonneuve et al., 2021). In general, a caldera cycle is accompanied by changes in the magma storage conditions, such as magma composition, physical properties of magma, and magma storage depth (Pabst et al., 2008; Forni et al., 2018; Metrich et al., 2018; Bouvet de Maisonneuve et al., 2021). Pattern of changes in magma storage conditions of some volcanoes, which have more than one caldera cycle, has been well known, such as Campi Flegrei-Italy (Forni et al., 2018), Rinjani-Indonesia (Vidal et al., 2015; Métrich et al., 2017), and Aso-Japan (Miyabuchi, 2009; Keller et al., 2023). A better understanding about these patterns is important to identify the past and present conditions as a key to determining hazardous behavior and forecast future potential hazards.

A recent study of Ismail et al. (2020) used these events to separate three eruptive periods of Krakatau, namely, Old Krakatau, Young Krakatau, and Anak Krakatau. The activities until CFE AD 416 are referred to the Old Krakatau period. Meanwhile, the activities after AD 416 until CFE 1883 are called the Young Krakatau period and the activities after CFE 1883 until present are Anak Krakatau period. Previous petrological and geochemical studies of Krakatau have not investigated the Old Krakatau eruptive products, focusing mainly on the products of the late Young Krakatau period (1883) and Anak Krakatau. An overview of these and our studies are listed in the Supplementary Table S1.

In this study, we covered some of the volcanic products from ancient (Old Krakatau) to recent (Anak Krakatau) to identify possible changes in the magma storage conditions within the Krakatau plumbing systems, as this information is required for monitoring and hazard assessment. We used a combination of petrological, geochemical, and rock magnetic analyses, which are standard tools for characterizing volcanic products (Cañón-Tapia and Pinkerton, 2000; Cinku et al., 2009; Ferré et al., 2012; Amor et al., 2019; Haag et al., 2021; Lerner et al., 2022). We also present mineralogical data, phenocryst and matrix glass compositions to reveal the magmatic plumbing systems, including the storage pressures and/or temperatures from the ancient (Old Krakatau) to the most recent (Anak Krakatau) periods.

Apart from plagioclase and pyroxene, we present mineralogical (including textural) and geochemical data of magnetic minerals. Magnetic minerals are sensitive to magma composition and differentiation, oxidation state, pressure, and temperature (Buddington and Lindsley, 1964; Haggerty, 1991; Lanza and Meloni, 2006; Mollo et al., 2013; Liao et al., 2016; Anai et al., 2023). Therefore, previous researchers have reported that magnetic mineral characteristics, such as abundance, composition, texture, and grain size can reflect magmatic conditions and processes (Mollo et al., 2013; Lerner et al., 2022; Xu et al., 2022). The characteristics of magnetic minerals can be identified by geochemistry, petrology, and rock magnetic methods. Rock magnetic properties (magnetic susceptibility, magnetic hysteresis properties, and Curie temperature) are proxies for magnetic mineral characteristics (Nagata, 2013; Pratama et al., 2018; Lerner et al., 2022). Combining these data (common minerals, matrix glass, and magnetic mineral characteristics) can provide comprehensive insights to reveal magma storage conditions.

Since this research is the first to be performed at Krakatau volcano covering all eruptive periods, this study provides: 1) a preliminary view on the characteristics of eruptive products and magma storage conditions during the earlier period of Krakatau, which is still undetermined; and 2) an overview of the magmatic evolution of several units from Old Krakatau to Anak Krakatau. In addition, the results of this study can serve as a basis for understanding the caldera cycle of the Krakatau system and also for other volcanoes that have experienced a similar evolution, where caldera-forming eruptions have occurred twice, i.e., at the end of the Old Krakatau and Young Krakatau periods. By knowing the pattern of the caldera cycle at Krakatau, the changing of the unrest state can be interpreted with greater confidence in relation to eruptive activity (Bouvet de Maisonneuve et al., 2021).

2 Geological background

Krakatau volcano is located 141 km northeast of the Sunda Trench, between Java and Sumatra Islands, and belongs to the Sunda Volcanic Arc, where the Indo-Australian Plate subducts beneath the Eurasian Continent (Figure 1). As mentioned above, the Krakatau Volcano activities are divided into three eruptive periods (i.e., Old Krakatau, Young Krakatau, and Anak Krakatau).

The Old Krakatau period is assumed to begin before AD 416 (Stehn, 1929; Bronto, 2000; Winchester, 2003). Meanwhile, the eruption center in this stage was the ancient Krakatau (Ismail et al., 2020). The eruptive products of Old Krakatau consist of dacitic lava flows, a pyroclastic fall, and pyroclastic flows (Stehn, 1929; Gardner et al., 2013; Abdurrachman et al., 2018), where the latter were associated with the first CFE (Ismail et al., 2020). Most lava and pyroclastic flow deposits are found on all three islands, whereas the pyroclastic fall deposit was found on the southern Panjang Island. The Old Krakatau period ended with the first CFE destroying the initial Krakatau edifice (Sutawidjaja, 2006), to form three islands: Panjang, Sertung, and Rakata (Francis, 1985).

After the first CFE, and at the start of Young Krakatau period, eruptive activity resumed on Rakata Island producing a pyroclastic fall. While no eruptive activity continued on Panjang and Sertung islands, Rakata Island kept growing, formed by alternating lava flows and pyroclastic falls. Danan and Perbuatan cones were subsequently formed. The eruptive products from Rakata and Danan-Perbuatan series were dominantly andesitic lavas (Westerveld, 1952; Camus et al., 1987). However, basaltic and andesitic dykes also occurred on Rakata (Camus et al., 1987). There were three eruption centers during this period: Rakata, Danan, and Perbuatan (Francis, 1985). Subsequently, the second CFE (VEI = 6) occurred in 1883,

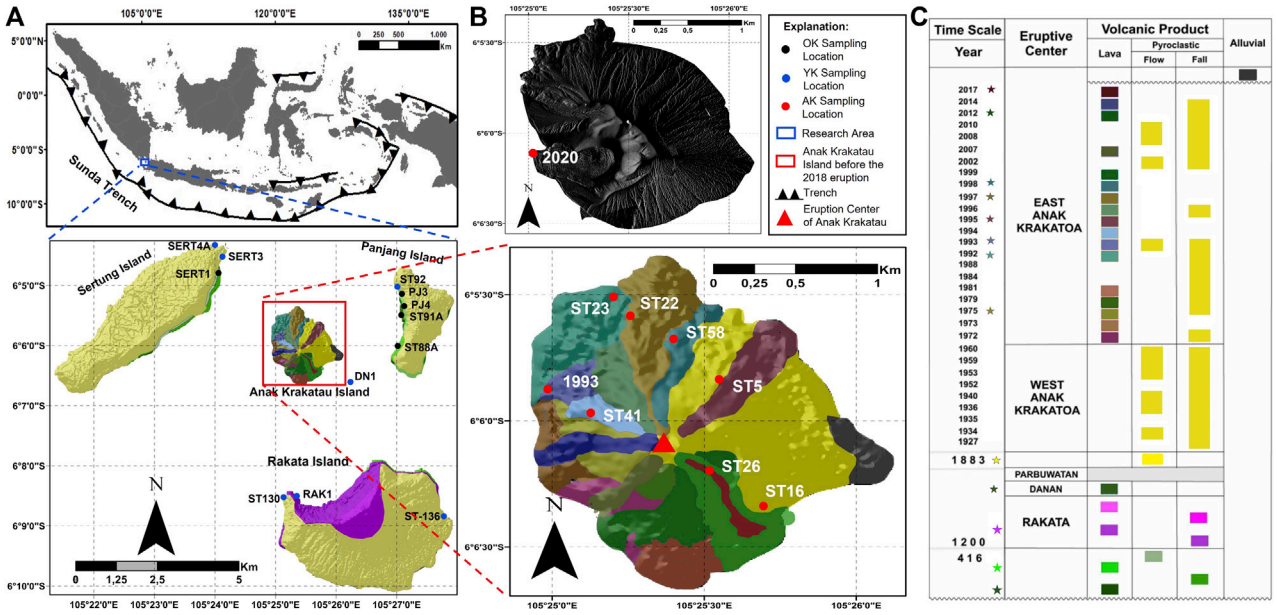

FIGURE 1
(A) Sample locations and volcanostatigraphy of Krakatau before the 2018 eruption. An overview of the remaining body of the Danan cone can be seen in Figure 2D. **(B)** A Topographic map of Anak Krakatau in 2021 and the location of lava samples collected in 2020. **(C)** The volcanostratigraphy of Krakatau. The unit names can be seen in Table 1. Stars indicate the samples collected and analyzed (modified after Abdurrachman et al., 2018). OK = Old Krakakatu, YK = Young Krakatau, AK = Anak Krakatau.

destroying Rakata, Danan, and Perbuatan and caused a tsunami that killed more than 36,000 people (Simkin and Fiske, 1983; Maeno and Imamura, 2011; PVMBG, 2014; Mutaqin et al., 2019). This second CFE produced pyroclastic deposits generally >10 m thick, that are found on Panjang, Rakata, and Sertung islands (Madden-Nadeau et al., 2021) and marked the end of Young Krakatau period.

In 1927, a new cone named Anak Krakatau emerged from the sea (Stehn, 1929; Self and Rampino, 1981; Self, 1992; Mandaville et al., 1996), which started the Anak Krakatau period. It was followed by both explosive and effusive eruptions that continue to the present day (Gardner et al., 2013; Abdurrachman et al., 2018). Most of the Anak Krakatau eruptive products are basaltic to andesitic lava flows and volcanic bombs (Westerveld, 1952; Camus et al., 1987; Dahren et al., 2012). The most significant activity during the past few years was the 2018 eruption that generated landslides due to volcanic flank failure and caused tsunamis that hit the southeast coast of Sumatra and west of Java killing more than 400 people (Muhari et al., 2019; Walter et al., 2019; Novellino et al., 2020; Ye et al., 2020; Grilli et al., 2021; Hunt et al., 2021; Cutler et al., 2022). However, Anak Krakatau continues to grow, and its recent eruptions mostly produce lava flows and volcanic ash (PVMBG, 2022).

3 Fieldwork and sample descriptions

We collected 16 samples of lava and 5 of pumice as listed in Table 1. The samples of this study do not fully represent the complete units of Krakatau systems as described by Ismail et al. (2020). We could not collect: 1) The pyroclastic fall (KTJP) and flow (KTAP) units from Old Krakatau; and 2) two pyroclastic fall units (RKJP1 and RKJP2) and the lava unit of RKRAB of Rakata products from Young Krakatau, since all of these units are found in the bottom part of Rakata's inner wall/cliff face, adjacent to the sea surface, restricting us to collect them except by approaching them by swimming and/or climbing. In particular, for Anak Krakatau, we have selected nine samples (Table 1) covering the beginning, middle, and latest units. However, the samples cover all three eruptive periods, namely, Old Krakatau, Young Krakatau, and Anak Krakatau.

Notably, the majority of samples are lavas, with the exception of pumices from the Young Krakatau period, originating from the 1883 pyroclastic density current deposit. Old Krakatau samples are all lavas and come from different units, which are classified as KTL1 and KTL2 (Ismail et al., 2020). KTL1 is represented by samples ST88B, ST91A, PJ3, and PJ4, while KTL2 is represented by SERT1. Young Krakatau samples are represented by the Rakata lava (RAK1), Danan lava (DN1), and pumice samples from the KMAP unit of 1883 eruption (SERT3, SERT4, ST136, ST130, and ST 92). All samples were collected during our field trip in March 2017, excluding the 1993 and 2020 lava samples which were collected in June 2021 and December 2020, respectively. The relative age of the samples from Old Krakatau and Young Krakatau products was obtained from previous studies (Table 1), while distinguishing each lava flow (from 1984 to 2017) on Anak Krakatau was approached through digitizing Landsat imagery from Google Earth (Ismail et al., 2020).

The Old Krakatau lava outcrops have massive and platy joint structures (PJ3) or are auto-brecciated (SERT1) (Figures 2A, B), whereas the Young Krakatau lavas are blocky (RAK1 and DN1) (Figures 2C, D) and Anak Krakatau lavas are dominantly auto-brecciated (Figure 2F). Sample locations in the lava flow outcrop were selected based on the freshness of the samples and their

TABLE 1 List of studied samples. An 'x' symbol represents age information. [1]Stehn (1929), [2]Bronto (2000), [3]Winchester (2003), [4]Sutawidjaja (2006), [5]PVMBG (2014), [6]Google Earth, [7]Effendi et al. (1983), and [8]Yokoyama et al. (1983). N.C. = not collected. N.A. = not analyzed.

Eruptive product/Year of eruption	Unit (Ismail et al., 2020)	Sample Code	Sampling location	Age comparison							
				Relative							Absolute
				1	2	3	4	5	6	7	8
OK/?	KTL1	ST91A	Panjang	x	x	x					
	KTL1	ST88B	Panjang	x	x	x					
	KTL1	PJ3	Panjang	x	x	x					
	KTL1	PJ4	Panjang	x	x	x					
OK/?	KTJP	N.C.									
OK/?	KTL2	SERT1	Sertung	x	x	x					
OK/416?	KTAP	N.C.									
YK/?	RKJP1	N.C.									
YK/?	RKLB	RAK1	Rakata	x	x	x					
YK/?	RKJP2	N.C.									
YK/?	RKRAB	N.C.									
YK/?	DNAL	DN1	Danan							x	
YK/1883 Pumice	KMAP	SERT3	Sertung	x	x	x				x	x
	KMAP	SERT4	Sertung	x	x	x				x	x
	KMAP	ST136	Rakata	x	x	x				x	x
	KMAP	ST130	Rakata	x	x	x				x	x
	KMAP	ST92	Panjang	x	x	x				x	x
AK/1972	AKL1	N.C.									
AK/1973	AKL2	N.A.									
AK/1975	AKL3	ST41	Anak Krakatau				x	x			
AK/1979	AKL4	N.C.									
AK/1981	AKL5	N.A.									
AK/1992	AKL6	ST23	Anak Krakatau				x	x	x		
AK/1993	AKL7	1993	Anak Krakatau				x	x	x		
AK/1994	AKL8	N.C.									
AK/1995	AKL9	ST5	Anak Krakatau						x		
AK/1996	AKL10	N.C.									
AK/1997	AKL11	ST22	Anak Krakatau						x		
AK/1998	AKL12	ST58	Anak Krakatau						x		
AK/1999	AKL13	N.A.									
AK/2007	AKL14	N.A.									
AK/2012	AKL15	ST16	Anak Krakatau						x		
AK/2014	AKL16	N.A.									
AK/2017	AKL17	ST26	Anak Krakatau						x		
AK/2020	Recent	2020	Anak Krakatau						x		

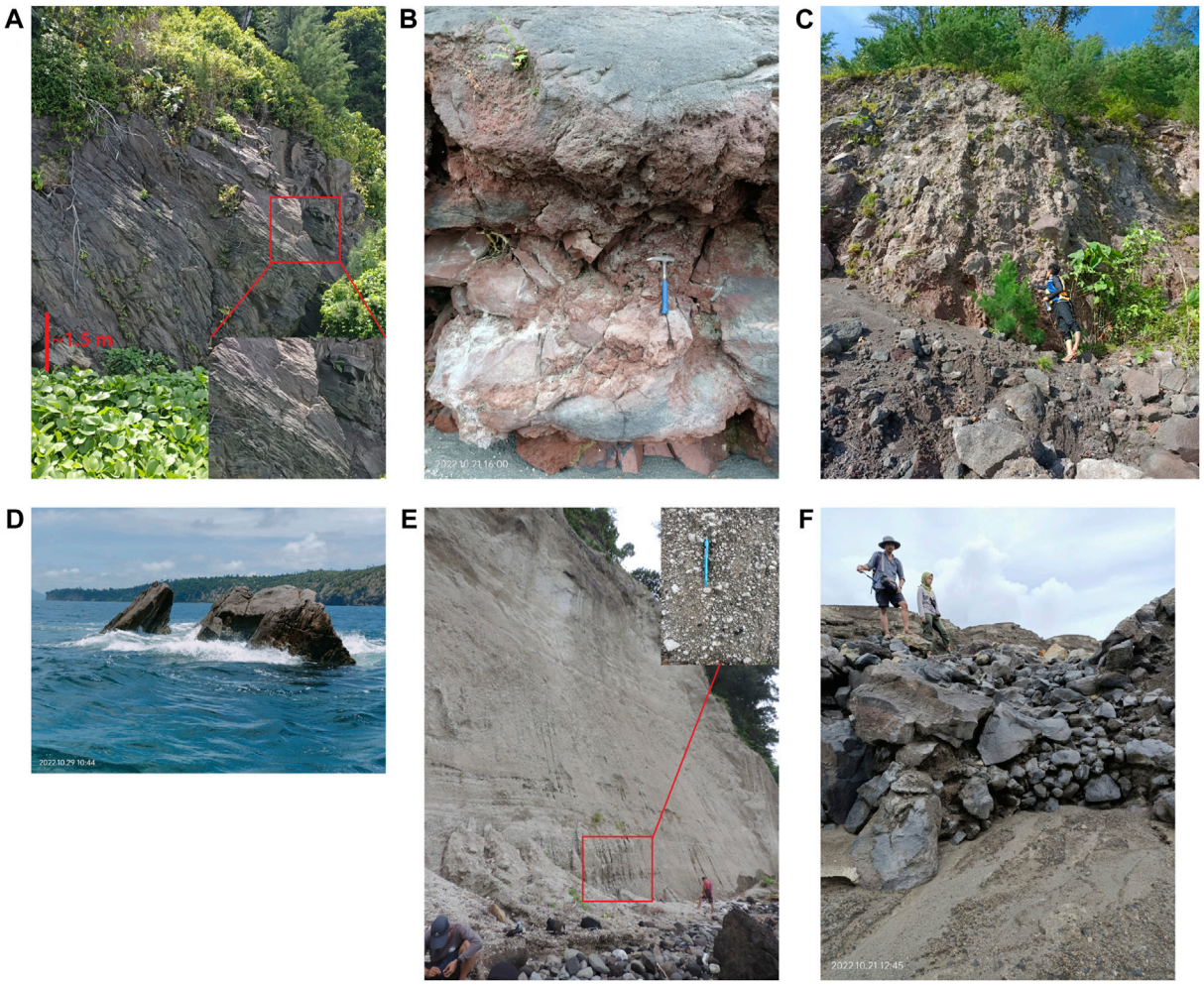

FIGURE 2
Representative products of each eruptive period: **(A)** lava PJ3, with massive blocky and platy joint structures (Old Krakatau) from Panjang island, **(B)** auto-brecciated lava SERT1 from Sertung island, blocky lava samples **(C)** RAK1, from Rakata island, and **(D)** DN1, from remaining body of Danan cone above sea level, **(E)** 60 m-thick pyroclastic flow deposits (sample ST92; Young Krakatau) observed on Panjang island, and **(F)** "a" ā lavas of sample ST41 on Anak Krakatau. See Figure 1 for the deposit locations.

availability in the field, as some surfaces were covered by the products of the 1883 eruption and recent volcanic ash. All of the sample locations can be seen in Figure 1. At Anak Krakatau itself, samples were collected on its edifice (mostly in the slope of Anak Krakatau) (Figure 1B bottom). Pumices from the Young Krakatau period were collected from ~25 to 30 m-thick pyroclastic deposits which outcropped up to 500 m in width, parallel to the shoreline. The deposits were dominantly composed of pumices, with less lithic and obsidian fragments ranging from lapilli to bomb sizes (Figure 2E). Representative photographs of hand samples can be seen in Supplementary Figure S2.

4 Materials and methods

All the analyses, as listed below, were performed for six samples representing each period: 1) Old Krakatau: PJ3 and SERT1, 2) Young Krakatau: RAK1, DN1, and SERT3, and 3) Anak Krakatau: 2020. Those representative samples come from different units within each period, and most of these samples have not been analyzed by previous studies. In addition, one sample from AK (2020) was chosen as it is the most recent product in our collection, for comparison to older Anak Krakatau eruptive products from previous studies. The analyses carried out on the rest of samples are listed in Supplementary Table S2.

4.1 Petrography

Petrographic analysis was done using an optical microscope, including phenocryst and groundmass observations to determine the textures and mineral associations of each sample.

4.2 Whole-rock geochemistry

All samples were ground to 200-mesh (<75 micron) powders. The freshness of samples was assessed using LOI (loss on ignition) measured on the dry powder samples using a Carbolite HTF High

Temperature Chamber Furnace (Carbolite Gero, United Kingdom) at the Research Centre for Geotechnology, National Research and Innovation Agency of Republic Indonesia (Badan Riset dan Inovasi Nasional - BRIN). LOI measurements were carried out twice on each sample and averaged. About 1 G of sample was heated to 105°C–110°C and then placed in a porcelain bowl whose weight was already known. It was heated to 400°C for 30 min before the temperature was increased to 1,000°C and left for 20 min. Afterwards, the sample was cooled in a desiccator vacuum for 20 min, then weighed. Whole-rock geochemistry was analyzed using a PUMA S2 XRF (X-ray fluorescence) (Bruker Corp., Massachusetts, United States) with a high power 50-W X-ray tube with a maximum current of 2 mA and accelerating voltage of 50 kV at the Research Centre for Chemistry, BRIN.

4.3 Minerals and matrix-glass compositions

Mineral and matrix-glass compositions of representative samples were analyzed with a JEOL JXA-ISP100 Super-probe EPMA in the Engineering Research Innovation Centre (ERIC), Engineering Faculty, Universitas Gadjah Mada, Indonesia. We obtained orthopyroxene, clinopyroxene, and matrix-glass compositions in the six representative samples listed. We used an accelerating voltage of 15 kV, probe current of 12 nA, and 1 μm beam diameter. Standard natural mineral samples of MAC 15298 and 15299 were used as standards for the quantitative chemical analysis. The results were processed with the ZAF correction method.

4.4 Geothermobarometry

To estimate the crystallization pressures and temperatures of minerals, and hence to infer magma storage locations and conditions, we used the orthopyroxene-liquid and two-pyroxene thermobarometry of Putirka (2008). We performed orthopyroxene-liquid thermobarometry on samples SERT1, DN1, and SERT3, where the pressures were estimated from a simple barometer using global calibration model for felsic liquid (excel spreadsheet can be downloaded from https://csm.fresnostate.edu/ees/faculty-staff/putirka.html). The standard error of estimate (SEE) for the global calibration is 320 MPa. We also applied two-pyroxene thermobarometry to sample PJ3 and the 2020 sample, where the pressure and temperature estimates were obtained using equations 39 and 36 of Putirka (2008), respectively. The SEE of these pressure and temperature estimates is ± 280 MPa and ± 45°C, respectively. For sample RAK1, we used the clinopyroxene-liquid thermobarometry of Putirka (2008).

4.5 Textural and composition analyses of magnetic minerals (Fe-Ti oxides)

We obtained back-scattered electron (BSE) images of gold-coated and polished resin mount of all samples using a Phenom ProX Desktop Scanning Electron Microscopy (SEM) at Geostech, Puspiptek, BRIN to identify the texture and the abundance of magnetic minerals. The magnetic mineral abundances were estimated using Olympus Stream Software by analyzing BSE images with an image depth of 96 dpi, a resolution of 4096 × 4096, and minimum size for particle recognition of 10 pixels. The compositions of magnetic minerals were determined using energy dispersive X-ray spectroscopy (EDS) on the SEM operating with an accelerating voltage of 15 kV and a full Backscattered Electron Detector (BSD).

4.6 Rock magnetic characteristics

We measured two rock magnetism parameters using instrumentation available at our institution: 1) Specific mass magnetic susceptibility (MS) was measured using a Bartington MS2B and MS3 magnetic susceptibility system (Bartington Instrument Ltd., Witney, United Kingdom) at the Laboratory for Characterization and Modelling of Rock Physical Properties, Bandung Institute of Technology. This measurement for each sample was done for three sub-samples (e.g., sample-1A, sample-1B, and sample-1C) where each sub-sample was measured five times and then averaged and the standard deviation calculated; 2) Isothermal Remanent Magnetization (IRM) acquisition curves were obtained using a Dexing 250 Vibrating Sample Magnetometer (VSM) with an external magnetic of 100 Oe-21000 Oe at the Research Center for Physics, BRIN. The baseline of any deflection in the Magnetization (M) vs. Magnetic Field (H) curve was determined using the adjacent-averaging second derivative method with a specified smoothing window and threshold using OriginLab Software. Linear fitting of the baseline anchors clearly defines the saturated point where the curve and line intersect (saturation field).

Those methods can produce valuable data to identify the characteristics of magnetic minerals, especially to identify the type, composition, and amount of magnetic minerals (Chi and Dorobek, 2004; Liebke et al., 2011; Sakra et al., 2020; Kanamaru et al., 2022) because magnetic susceptibility and magnetic field saturation are dependent on those properties. The rock magnetism parameters come in to confirm the results of SEM-EDS observations, in order to get the comprehensive results regarding the detail of characteristics of magnetic minerals contained in the rock.

5 Results

5.1 Mineralogy

The six representative samples contain plagioclase, pyroxene, and Fe-Ti oxides as the most common minerals. The general petrographic features of Old Krakatau, Young Krakatau, and Anak Krakatau can be summarized as follows.

The products of Old Krakatau are represented by the samples of PJ3 (30% phenocrysts) and SERT1 (60% phenocrysts). Both samples have porphyro-aphanitic textures, with larger crystals in SERT1 than in PJ3. The maximum crystal sizes in PJ3 and SERT1 are 1 mm and 3 mm, respectively. The mineral association in Old Krakatau consists of plagioclase,

clinopyroxene, orthopyroxene, and Fe-Ti oxides, while the groundmass in both samples is microlite-rich and consists of pyroxene, Fe-Ti oxides, plagioclase, and silica minerals. Although the mineral associations in both samples are similar, some differences are observed, including: 1) the Fe-Ti oxides in PJ3 consist of both magnetite and ilmenite, while those in SERT1 consist dominantly of magnetite; 2) silica minerals were observed in the matrix glass of PJ3 (Supplementary Figure S3A); and 3) unzoned plagioclase textures were dominantly observed in PJ3, while oscillatory zoning and sieve texture are often observed in SERT1. We also observed symplectite textures in some pyroxene phenocrysts in both samples, which are surrounded by small crystals of magnetite and orthopyroxene (Supplementary Figures S3B, C).

The Young Krakatau products are represented by two lava samples, DN1 (55% phenocrysts) and RAK1 (40% phenocrysts), and one pumice sample, SERT3 (5% phenocrysts). The lava samples have a porphyro-aphanitic texture, with phenocrysts reaching up to 4 and 5 mm in length in DN1 and RAK1, respectively. The pumice sample is dominated by volcanic glass and microphenocrysts <1 mm in length. Mineral associations in Young Krakatau lavas consist of plagioclase, pyroxene, and Fe-Ti oxides, while Young Krakatau pumice sample consists of plagioclase, orthopyroxene, and Fe-Ti oxides. Orthopyroxene and clinopyroxene are present as phenocrysts in DN1, but RAK1 is free of orthopyroxene, while SERT3 is free of clinopyroxene. Both magnetite and ilmenite exist in these three Young Krakatau samples. The groundmass of the lava samples is microlite-rich, consisting of plagioclase, pyroxene, Fe-Ti oxides, and silica minerals (predominantly in DN1), while the pumice is microlite poor. The silica minerals in Young Krakatau lava are less abundant compared to those found in Old Krakatau products. Normal zoning patterns in plagioclase dominate the Young Krakatau products. However, some oscillatory zoning and sieve textures are present in SERT3 and DN1. Symplectite textures occur in the pyroxene and magnetite phenocrysts in DN1, which are surrounded by small crystals of orthopyroxene.

Anak Krakatau is represented by recent lava that erupted in 2020, which also has porphyro-aphanitic texture with 60% phenocrysts with maximum lengths of 3 mm. The mineral association in Anak Krakatau consists of plagioclase, clinopyroxene, orthopyroxene, Fe-Ti oxides, and olivine. The matrix glass is rich in microlites consisting of pyroxene, Fe-Ti oxides, and plagioclase. Unlike older Krakatau products, no silica minerals were found in the AK groundmass. Fine and coarse sieve textures are common in the plagioclase crystals. Symplectite textures are infrequent in the pyroxene phenocrysts.

5.2 Whole-rock and matrix-glass geochemistry

Whole-rock compositions and LOI values of all samples are shown in Table 2. The samples are mostly fresh (little-to-no apparent weathering) as shown by LOI values of <1% (Tugrul and Gurpinar, 1997; Pratama et al., 2018) except some Young Krakatau samples which are >4% LOI, in agreement with data obtained by Madden-Nadeau et al. (2021) in which they suspected the samples to be altered by seawater. However, we compare data from Mandeville et al. (1996) and Madden-Nadeau et al. (2021) with geochemistry data for our Young Krakatau samples.

The compositions of all Old Krakatau lava samples are dacitic, with SiO_2 contents of 63.6–68.5 wt%, while Young Krakatau lava samples (both RAK1 and DN1) are andesitic with SiO_2 contents of 61.2 wt% and 62.7 wt%, respectively, and all Anak Krakatau lava samples are basaltic in composition, with SiO_2 contents of ~48.6–50.8 wt% (normalized) (Table 2; Figure 3). The Young Krakatau pumice samples are all dacitic with SiO_2 contents of 65.0–67.6 wt%. The mafic Anak Krakatau lavas are characterized by high Al_2O_3, FeO* (total iron as FeO), MgO, and CaO contents and slightly higher TiO_2 contents. In contrast, these major elements have low contents in Young and Old Krakatau lava samples (Supplementary Figure S4). However, the Young and Old Krakatau lavas can still be distinguished by their major element compositions. Figure 3 also shows that our Young Krakatau compositions are close to that of the 1883 pumice and olive obsidian presented by Mandaville et al. (1996), which are dacite to rhyolite, meaning that we obtained similar results despite our higher LOI values.

The matrix-glass major element compositions of representative samples from each period, normalized to 100% anhydrous, are listed in Supplementary Table S3. Matrix-glass compositions of these samples range from dacite to rhyolite, i.e., 66.3–78.8 wt% of SiO_2 (Figure 3). Despite being basaltic in composition, Anak Krakatau products have evolved matrix-glass compositions of 66.3–69.2 wt% SiO_2 (trachydacite). Young and Old Krakatau products have rhyolitic compositions, with SiO_2 contents of 70.6–78.8 wt% and 74.9–77.5 wt%, respectively. Binary plots of major element oxide contents of the matrix glasses of representative samples from each period show clear differentiation trends between Old Krakatau, Young Krakatau, and Anak Krakatau (Supplementary Figure S4).

5.3 Mineral chemistry

5.3.1 Pyroxene

The pyroxene compositions of six representative samples from each period are displayed in Figure 4A and tabulated in Supplementary Table S4. Clinopyroxene crystals in these samples are generally augite, while orthopyroxene is classified as pigeonite and enstatite. To identify distinct compositional groups, the FeO/MgO ratios and contents of selected major elements of clinopyroxene and orthopyroxene crystals were used.

5.3.1.1 Clinopyroxene

The major element compositions of clinopyroxene phenocrysts show three distinct compositional groups (Figure 4B). The first group, characterized by high FeO/MgO ratios (>0.9), narrow ranges of TiO_2 (0.4–0.5 wt%) and Al_2O_3 (1.1–1.5 wt%), and high MnO contents (>0.9 wt%), is represented by Old Krakatau (PJ3). The second group, characterized by moderate FeO/MgO (0.6–0.7), a wide range of Al_2O_3 contents (1.5–2.6 wt%), and narrow range of TiO_2 (0.5–0.8 wt %) and MnO contents (0.5–0.8 wt%), is represented by Young Krakatau (RAK1, DN1) and Old Krakatau (SERT1). The third group, characterized by lower FeO/MgO ratios (0.5–0.6), lower MnO (0.4–0.6 wt%), and wider range of TiO_2 (0.5–0.9 wt%) and Al_2O_3 (1.9–3.2 wt%) contents, is represented by Anak Krakatau (2020).

TABLE 2 Whole-rock major element compositions and LOI of all samples.

Period	Product	Sample	SiO_2 (wt%)	TiO_2 (wt%)	Al_2O_3 (wt%)	FeO (wt%)	MnO (wt%)	MgO (wt%)	CaO (wt%)	Na_2O (wt%)	K_2O (wt%)	P_2O5 (wt%)	LOI (%)
OK	Lava	ST88B	67.07	0.60	16.77	4.70	0.10	1.20	2.31	3.92	2.41	0.40	0.20
	Lava	ST91A	66.80	0.60	16.80	4.89	0.10	1.11	2.21	4.02	2.41	0.50	0.50
	Lava	PJ3	68.20	0.60	15.85	4.15	0.10	1.81	2.21	3.91	2.21	0.50	0.01
	Lava	PJ4	67.97	0.60	16.16	3.98	0.10	1.51	2.11	4.32	2.31	0.50	0.003
	Lava	SERT1	63.18	0.91	17.30	5.61	0.20	1.91	4.02	3.82	1.81	0.60	0.005
YK	Lava	RAK1	60.83	1.01	18.23	5.89	0.20	2.11	5.14	3.73	1.61	0.60	0.01
	Lava	DN1	62.27	1.01	17.00	5.79	0.20	2.21	5.03	3.52	1.71	0.60	0.01
	Pumice	ST92	64.55	1.06	14.39	6.38	0.21	1.69	3.60	3.92	2.65	0.85	9.50
	Pumice	ST130	65.44	0.92	15.39	6.42	0.20	1.53	3.36	2.85	2.45	0.71	5.60
	Pumice	ST136	67.07	0.91	15.50	5.11	0.20	1.32	2.94	3.34	2.33	0.71	4.80
	Pumice	SERT3	67.24	0.81	16.17	4.12	0.20	1.63	2.75	3.87	2.24	0.51	0.03
	Pumice	SERT4	65.87	0.93	15.62	5.02	0.21	1.65	3.21	4.03	2.28	0.62	0.06
AK	Lava	ST41	50.25	1.21	21.21	9.59	0.20	3.92	8.24	3.02	0.80	0.50	0.20
	Lava	ST23	49.95	1.21	21.51	9.86	0.20	3.32	8.44	3.02	0.80	0.60	0.20
	Lava	1993	47.98	1.31	21.07	11.88	0.20	3.13	8.97	2.72	0.81	0.60	0.30
	Lava	ST5	50.05	1.21	21.31	9.59	0.20	3.72	8.54	3.02	0.80	0.50	0.20
	Lava	ST22	49.95	1.21	21.61	9.59	0.20	3.32	8.54	3.12	0.80	0.60	0.10
	Lava	ST58	49.85	1.21	21.41	9.68	0.20	3.92	8.24	3.02	0.80	0.60	0.10
	Lava	ST16	49.35	1.31	21.01	10.58	0.20	3.82	8.24	2.91	0.80	0.60	0.30
	Lava	ST26	49.24	1.11	22.05	9.51	0.20	3.63	8.86	3.12	0.70	0.50	0.30
	Lava	2020	48.94	1.31	20.95	11.15	0.20	3.22	8.76	2.72	0.91	0.60	0.10

5.3.1.2 Orthopyroxene

The major element compositions of orthopyroxene phenocrysts also showed three distinct compositional groups (Figure 4B). The first group is characterized by high FeO/MgO ratios (>1.1), a narrow range of TiO_2 contents (0.2–0.3 wt%), low Al_2O_3 contents (0.6 wt%), and high MnO contents (1.5–1.8 wt%), and is represented by Old Krakatau (PJ3). The second group, characterized by moderate FeO/MgO ratios (0.8–1), a narrow range of TiO_2 (0.2–0.4 wt%) and Al_2O_3 (0.6–1.1 wt%) contents, and wide range of MnO contents (1–1.9 wt%), is represented by all Young Krakatau (DN1, SERT3) and Old Krakatau (SERT1). The third group, characterized by lower FeO/MgO ratios (0.6–0.7), lower MnO contents (0.5-1 wt%), and narrow range of TiO_2 (0.2–0.4 wt%) and Al_2O_3 (1.1–1.4 wt%) contents, is represented by AK.

5.3.2 Fe-Ti oxides

The compositions of Fe-Ti oxides were measured in five samples from the Old Krakatau period (ST88B, ST91A, PJ3, PJ4, and SERT1), four samples from the Young Krakatau period (RAK1, DN1, ST92, and SERT3), and two samples from the Anak Krakatau period (ST41 and 2020). Their compositions can be seen in Supplementary Table S5 and are illustrated on the Fe-Ti-O ternary diagram shown in Figure 5A. In general, Figure 5A shows that the Fe-Ti oxides can be classified into two groups: 1) those that fall in or near the ilmenite-hematite solid solution line (titanohematite, TH-series), and 2) those that fall along the ulvöspinel-magnetite solid solution line (titanomagnetite, TM-series). Representative samples from each eruptive period have relatively distinct compositions in both series.

All the Fe-Ti oxides in Anak Krakatau samples are titanomagnetite, with molar fractions of ulvöspinel (X_{Usp}) of 0.26–0.49; however, Young and Old Krakatau samples contain both titanomagnetite and titanohematite/ferrian-ilmenite as distinct grains. Titanomagnetite grains in Young Krakatau samples have a similar range of X_{Usp} to those from Anak Krakatau, but the titanomagnetite in Old Krakatau samples has a wide range of X_{Usp} (0.24–0.85). The Old Krakatau samples have slightly higher molar fractions of ilmenite (X_{Ilm}; 0.87–1.00) than the Young Krakatau samples, although some Young Krakatau ilmenite overlaps those form Old Krakatau (Figure 5A). In addition, the compositions of the titanomagnetite and ilmenite in the Old Krakatau, Young Krakatau, and Anak Krakatau periods can be distinguished clearly, as shown in Figure 5B. Generally, the titanomagnetite TiO_2 and MnO contents decrease towards the younger samples, whereas the Al_2O_3 contents increase. Similar trends are observed in the ilmenite TiO_2 and MnO contents, but there is no clear trend in the ilmenite Al_2O_3 contents.

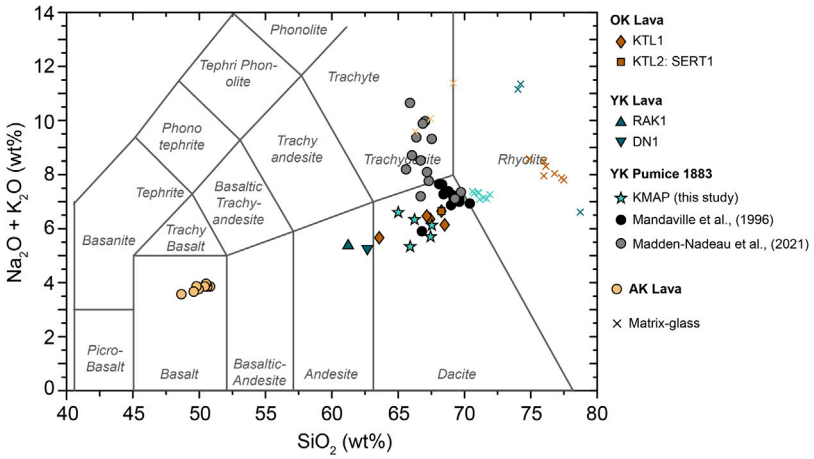

FIGURE 3
A total alkali-silica diagram (Le Bas et al., 1986), showing the whole-rock compositions of all samples and matrix-glass compositions (x symbols) of four samples: SERT 1 (brown), RAK1 (dark cyan), SERT3 (bright cyan), and 2020 (orange). OK = Old Krakatau, YK = Young Krakatau, AK = Anak Krakatau.

5.4 Pressure and temperature estimation

The presence of two pyroxenes in all Krakatau products allows the application of the pyroxene geobarometer of Putirka (2008). Equilibrium tests between orthopyroxene and liquid and between the two pyroxenes are shown in Supplementary Figures S5, S6, respectively. Orthopyroxene-liquid thermobarometry yields good K_D (Fe-Mg) values for some pyroxene compositions with Old and Young Krakatau matrix-glass and whole-rock compositions, although not for all Anak Krakatau samples. To convert the pressure to the depth of magma storage, we used a density of 2.55 gcm^{-3}, as also used by Mandeville et al. (1996) at Krakatau. The orthopyroxene-liquid geobarometer (Figure 6A) generally yields low pressures and shallow depths, i.e., 14–72 MPa (0.6–2.9 km) and 26–84 MPa (1.1–3.4 km) for Old Krakatau and Young Krakatau, respectively. Since we used the pressure from the global calibration of felsic liquids, which are not sensitive to temperature (T), we can only report the pressure data. For the Old and Anak Krakatau samples, we used two-pyroxene thermobarometry from Putirka (2008). We are unable to provide pressure and temperature estimates from the PJ3 sample due to the low Al_2O_3 content of the pyroxene (<1 wt%), which did not yield reasonable P and T values. Our Anak Krakatau samples are in equilibrium under subsolidus conditions, with K_D values close to 0.7. Two-pyroxene microphenocryst pairs yield pressures of 185–390 MPa (7.4–15.6 km; Figure 6B), with temperatures ranging of 916°C–956°C. Two-pyroxene phenocryst pairs yield high crystallization pressures, 428–665 MPa (17.1–26.6 km), with temperature ranging from 983°C to 1,034°C.

5.5 Magnetic mineral (Fe-Ti oxide) textures

Fe-Ti oxides minerals have magnetic properties that will be discussed in the following section. Not only does the chemical composition of the Fe-Ti oxides differ in each period, their textures also vary across the eruptive period. In general, both titanomagnetite and ilmenite phenocrysts and microlites are anhedral to subhedral (Figure 7).

In Old Krakatau samples, the grain boundaries of titanomagnetite crystals are often corroded while being surrounded by pyroxene or plagioclase microlites (Figures 7A, D). Figure 7A also shows an example of an ilmenite inclusion in the rim of a titanomagnetite crystal. This texture could represent composite-type exsolution (Buddington and Lindsley, 1964; Haggerty, 1991; Tan et al., 2016). In addition, ilmenite also occurs in Old Krakatau samples as a trellis-like lamellae with the width of about <5 μm, occupying more than 60% of the host area (Figure 7B), and appears as an individual grain (Figure 7C).

In the Young Krakatau samples, particularly in the lava samples, the titanomagnetite grain boundaries also appear to be corroded (Figures 7E, F). In addition, Figure 7E shows ilmenite exsolution lamellae included as a trellis type with a width of about 7.5 μm and covering about 22% of the host area. In pumice samples (ST92 and SERT3), both titanomagnetite and ilmenite crystals are generally subhedral, have sharp or smooth edges, and sometimes are embayed (Figures 7G, H, I). Figure 7G also shows the different colors of titanomagnetite (Tmt) and ilmenite (Ilm) in BSE images, where the latter tends to be darker.

Unlike the Old and Young Krakatau samples, the Fe-Ti oxides in the Anak Krakatau samples tend to be more anhedral and have a variety of textures, including graphic textures or myrmekite-like titanomagnetite (Figure 7J), small skeletal or hopper titanomagnetite microlites (Figure 7K), and ilmenite exsolution lamellae in titanomagnetite hosts (Figure 7L). These lamellae are trellis-like (Tan et al., 2016), with widths of about 5 μm and covering about <10% of the host area. In addition, coarse magnetic minerals ($\geq$ 2 μm) are more abundant in the Anak Krakatau sample (2020), while the Old Krakatau sample (ST91A) contained finer minerals ($\leq$ 2 μm) (Supplementary Figure S7). The mean size of magnetic minerals

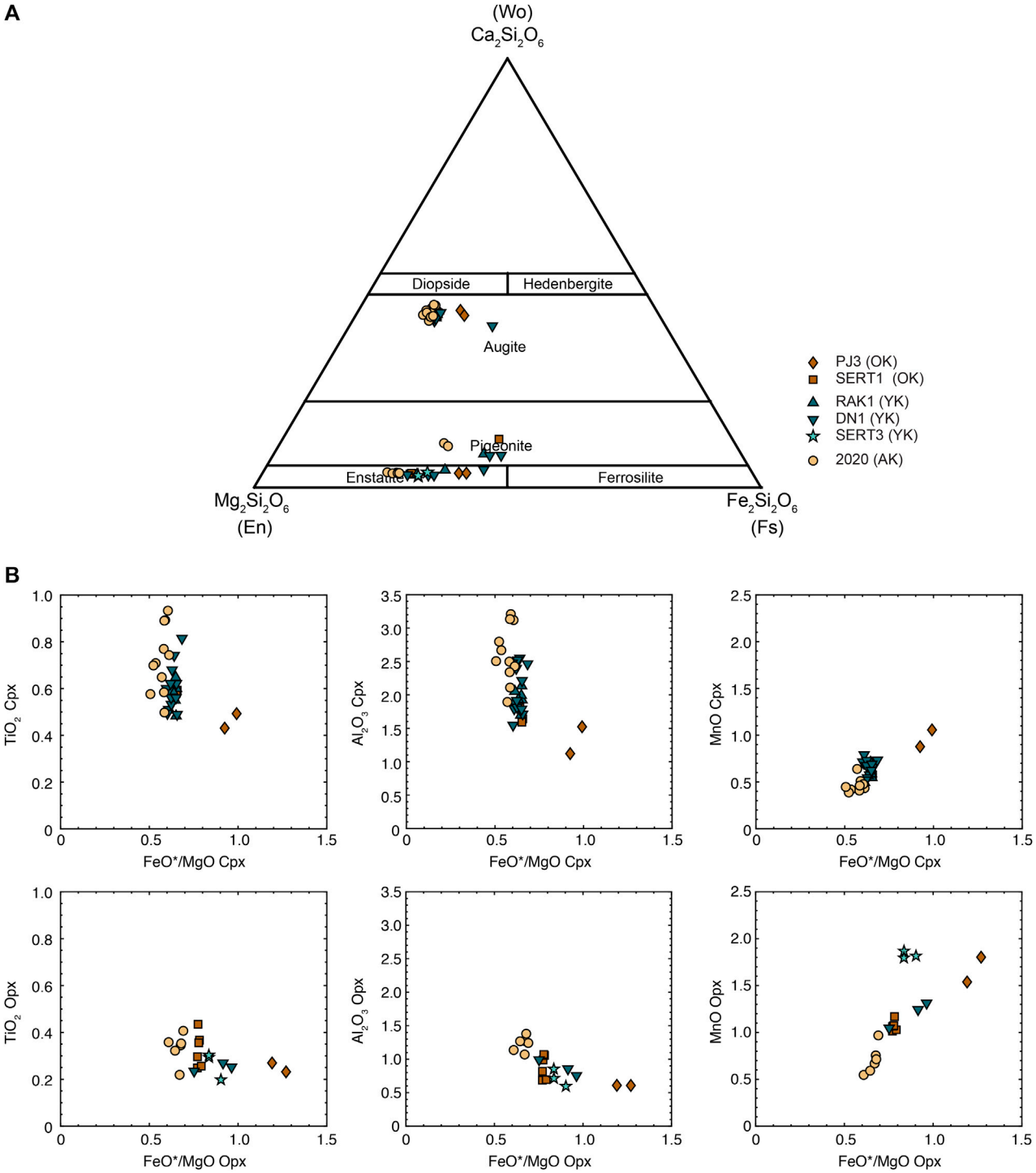

FIGURE 4
(A) A pyroxene ternary diagram and **(B)** the FeO(total)/MgO ratios of clinopyroxene and orthopyroxene versus selected major element oxides. OK = Old Krakatau, YK = Young Krakatau, AK = Anak Krakatau.

in the Young Krakatau pumice (ST92) is difficult to identify due to their sparse presence regarding the field of view. However, measurement from several SEM images shows that their sizes are ranging from ~10 to 200 μm. Overall, Anak and Old Krakatau samples contain magnetic minerals of 2.5% and 2% (by area fraction), respectively.

5.6 Rock magnetic properties

The rock magnetic analyses measured several parameters (Supplementary Table S7). The MS values of the Old Krakatau samples are lower than the Young and Anak Krakatau samples, between 273.33 × 10^{-8} m^3/kg to 632.99 × 10^{-8} m^3/kg, with a mean

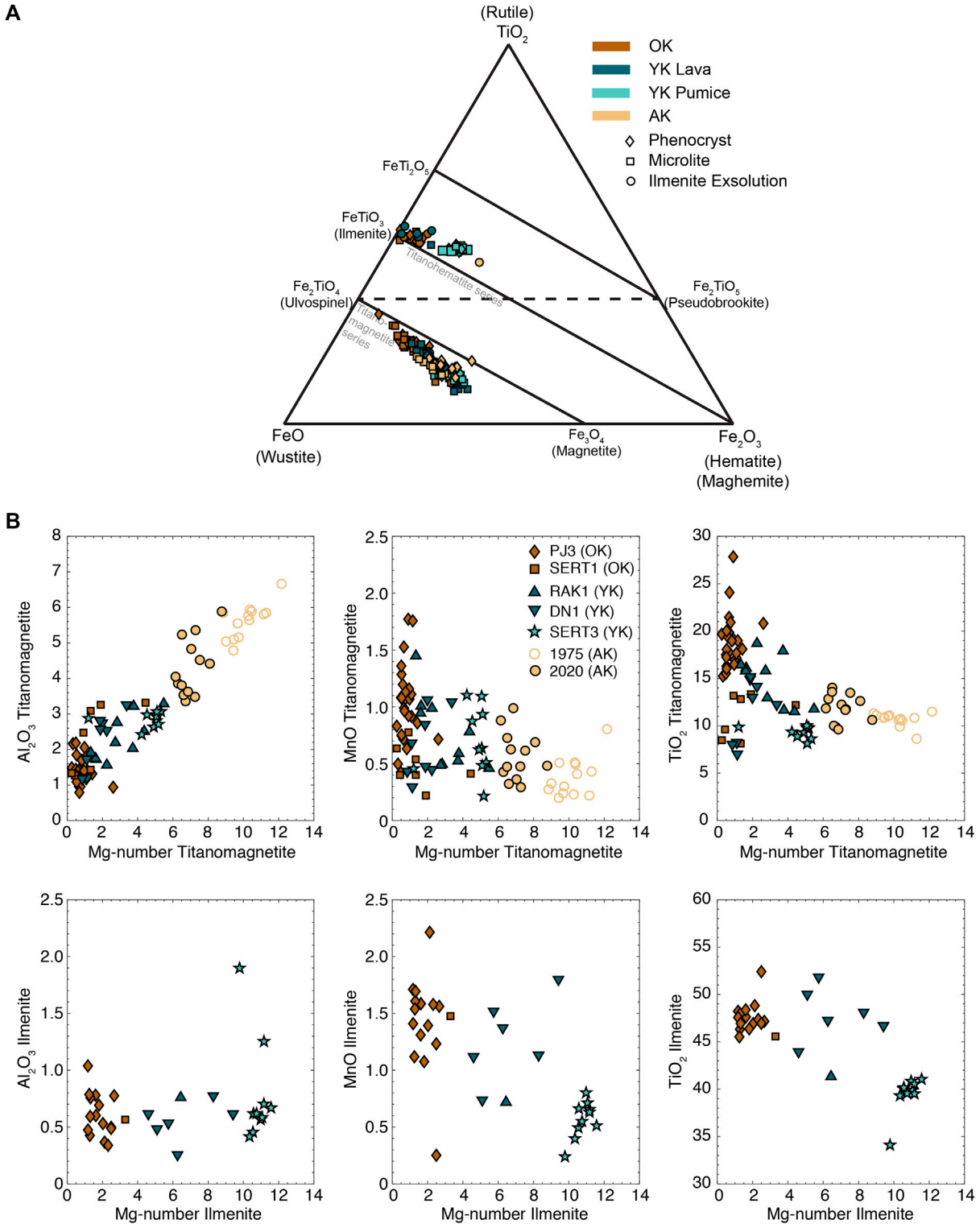

FIGURE 5
(A) An Fe-Ti-O ternary diagram showing the compositions of titanomagnetite and ilmenite crystals from representative samples from each eruptive period: Old Krakatau (ST88B, ST91A, PJ3, PJ4, SERT1); Young Krakatau lavas (RAK1 and DN1); Young Krakatau Pumices (ST92 and SERT3) and AK (ST41 and 2020). Fe_2O_3 was recalculated based on stoichiometry and charge balance and the Fe-Ti oxide compositions are tabulated in Supplementary Table S5. **(B)** Titanomagnetite and ilmenite Al_2O_3, TiO_2, and MnO contents versus Mg number. The Mg number was calculated following the approach of Keller et al. (2023).

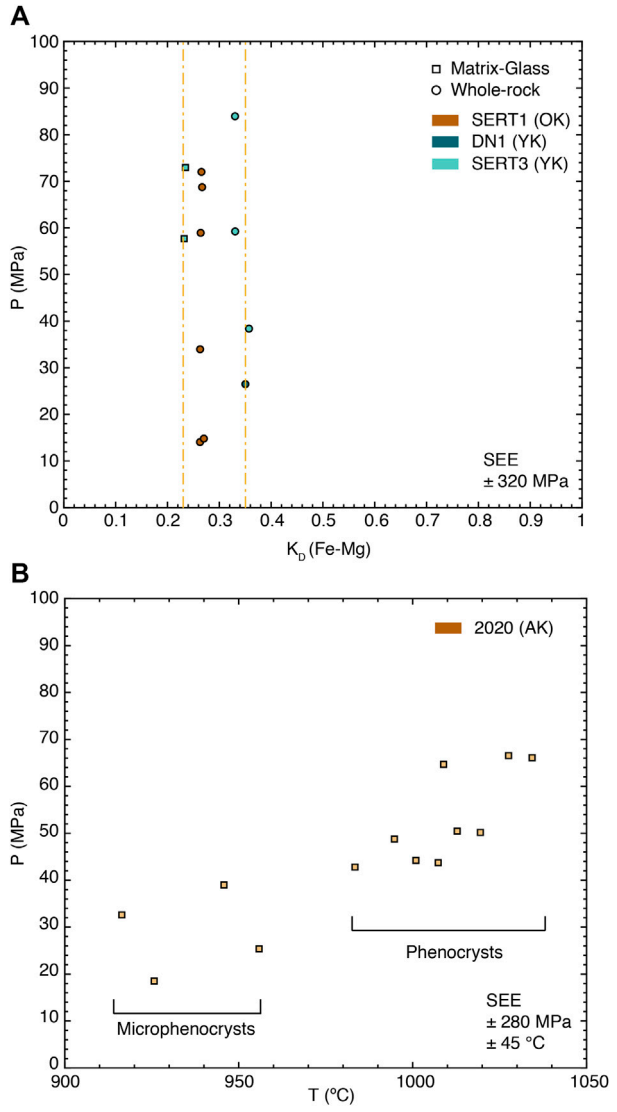

FIGURE 6
(A) Result of the orthopyroxene-liquid barometer using matrix-glass and orthopyroxene compositions of the lavas from SERT1 (Old Krakakatu), DN1 (YK), and pumice from SERT-3 (Young Krakatau). All samples yield relatively low pressures (14–84 MPa). **(B)** Pressure versus temperature diagram obtained from two-pyroxene geothermobarometry on the AK (2020) lava. Pyroxene microphenocryst pairs yield dominantly low crystallization pressures (185–390 MPa) and temperatures ranging from 916°C to 956°C. Two-pyroxene phenocryst pairs yield high crystallization pressures (428–665 MPa) and temperatures ranging from 983°C to 1,034°C. OK = Old Krakakatu, YK = Young Krakatau, AK = Anak Krakatau.

value of 443.05 × 10^{-8} m^3/kg (Figure 8A) The Young Krakatau pumice samples (ST92, ST130, ST136, SERT3, and SERT4), erupted during the catastrophic 1883 eruption, yield MS values of <500 × 10^{-8} m^3/kg (Figure 8A). The MS values of the Young Krakatau lava samples (DN and RAK1) are 765.57 × 10^{-8} m^3/kg and 1438.06 × 10^{-8} m^3/kg, respectively. The MS values of all AK samples are higher than 1,000 × 10^{-8} m^3/kg, higher than those of the Young Krakatau and Old Krakatau samples.

The results of magnetic field saturation of all the samples are listed in Supplementary Table S6 and visualized in Figure 8B. Figure 9 shows the IRM acquisition curves of representative samples. Each sample was saturated at different values, indicated by the vertical dashed lines. For example, sample PJ4 (Old Krakatau) had the highest saturation value (~576.77 mT). The Young Krakatau samples, represented by lava RAK1 and pumice ST92, were saturated at about 480.00 and ~510.09 mT, respectively, lower than the Old Krakatau sample. Sample ST22 (AK) saturated early, at ~404.52 mT. O'Reilly (1984) showed that the saturation magnetization field for pure magnetite is about 300 mT, whereas all our samples have saturation magnetization field values above 300 mT (Figure 8B, Supplementary Table S6). This indicates that the magnetic minerals in the samples are a mixture of Fe-rich and Ti-rich titanomagnetite or high coercivity magnetic minerals (Chi and Dorobek, 2004; Liebke et al., 2011; Pratama et al., 2018). Furthermore, the saturation magnetization fields of the Old Krakatau samples are higher than those of the Young and Anak Krakatau samples, indicating that the Old Krakatau samples contain more heterogeneous magnetic minerals.

6 Discussion

We summarize the view of Krakatau plumbing systems during the Old Krakatau, Young Krakatau, and Anak Krakatau periods, inferred from their whole-rock and glass compositions, mineral chemistry, geothermobarometry, and magnetic mineral properties and textures. This study is the first to report a view of Old Krakatau that can serve as a basis for future research. However, we used limited samples from the Old, Young, and Anak Krakatau periods. Particularly for Old Krakatau, products from CFE were not included in our study. The whole-rock and glass compositions show the evolution of Krakatau magmas. Our samples are free from hydrous minerals, e.g., biotite and amphibole, and the most common phases that track chemical variations within the anhydrous reservoirs are plagioclase and pyroxene (Keller et al., 2023). These two minerals often have strong chemical zonation, therefore their chemical composition tends to change and may not be suitable for performing mineral thermobarometry (Keller et al., 2023). In our samples, the pyroxene crystals are less zoned than the plagioclase crystals, hence we chose to use pyroxene compositions as a proxy to detect variations in the magma that show the evolution of the magma across the period, and also to estimate the magma storage pressures and temperatures during each period. In addition, Fe-Ti oxides are abundant in our samples, where they (particularly titanomagnetite) can serve as ideal tracers of the average chemical differences in eruptive products (e.g., Bouvet de Maisonneuve et al., 2021; Keller et al., 2023). We combine their compositions and textures to provide information on magma differentiation and evolution as well as on the magma conditions (e.g., oxygen fugacity, fO_2). We also relate the composition of the Fe-Ti oxides to their magnetic properties, as iron (Fe) is one of the main elements that can carry magnetic moments.

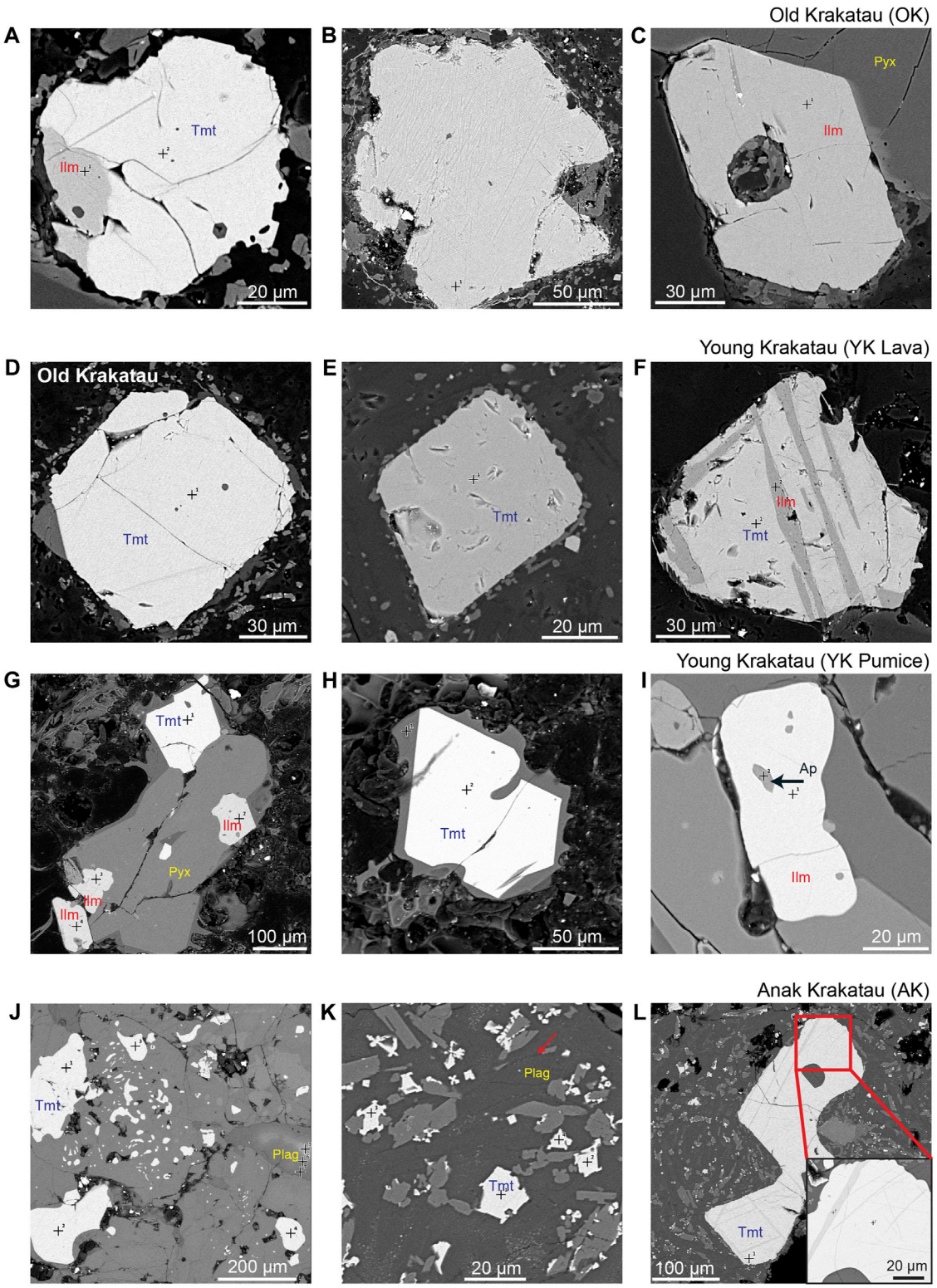

FIGURE 7
BSE images of magnetic minerals/Fe-Ti oxides in representative samples from each eruptive period. **(A)** Ilmenite (Ilm) inclusion in the rim of a titanomagnetite (Tmt) crystal. **(B)** Trellis-like exsolution lamellae in a titanomagnetite host. **(C)** Ilmenite microphenocryst. **(D–E)** Corroded grain boundaries of titanomagnetite surrounded by glass and microlites of pyroxene or plagioclase. **(F)** Ilmenite exsolution lamellae in a titanomagnetite host. **(G)** Pyroxene (Pyx)-titanomagnetite-ilmenite intergrowth. The upper titanomagnetite and lower left ilmenite are embayed. **(H)** An embayed titanomagnetite surrounded by glass. **(I)** Ilmenite hosting apatite (Ap) inclusions. **(J)** A graphic titanomagnetite in ST41. All white crystals are titanomagnetite. **(K)** Skeletal titanomagnetite microlites in the 2020 sample. The red arrow shows matrix glass that is indicated by the darker gap area between plagioclase crystals (plag). **(L)** Trellis-like exsolution lamellae in a titanomagnetite host.

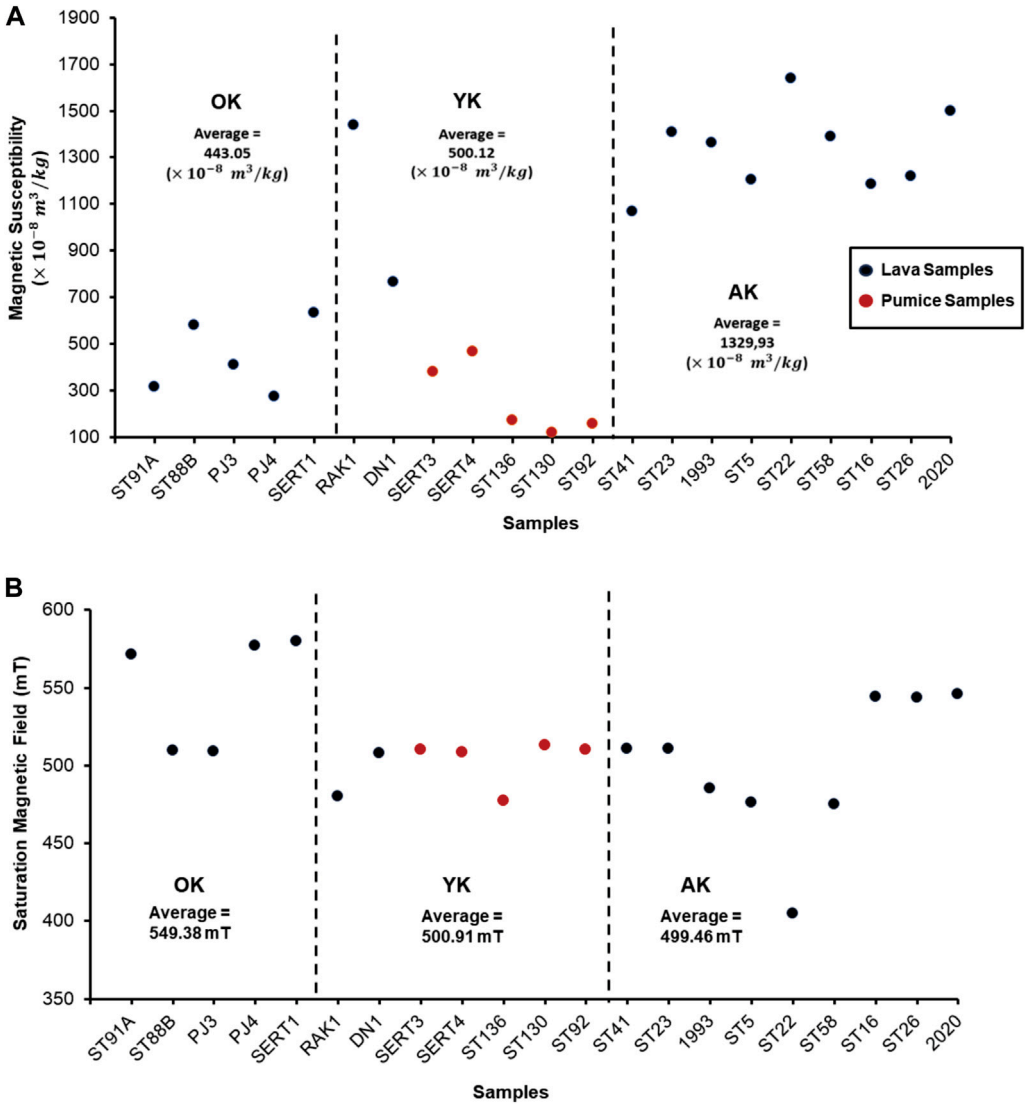

FIGURE 8
Plot of **(A)** Magnetic susceptibility and **(B)** Saturation magnetic field for all samples. OK = Old Krakatau, YK = Young Krakatau, AK = Anak Krakatau.

6.1 Magma storage conditions during the different eruptive periods

6.1.1 Old Krakatau

The whole-rock and glass chemical compositions of the Old Krakatau samples are the most evolved among all the eruptive periods, which indicates a higher degree of magma differentiation. These evolved compositions are consistent with 1) the highest clino- and orthopyroxene FeO/MgO ratios and 2) the highest titanomagnetite MnO/Al_2O_3 ratios and lowest titanomagnetite Mg numbers (Figure 10A). SERT 1 (KTL2) is not as evolved as PJ3 (KTL1), as shown by the lower clino- and orthopyroxene FeO/MgO ratios (Figure 4B) and lower titanomagnetite MnO/Al_2O_3 ratios (Figure 10A). The MnO/Al_2O_3 ratio (Mn is highly incompatible, whereas Al is highly compatible) can be used as a differentiation index, where higher MnO/Al_2O_3 ratios indicate higher degrees of differentiation (Keller et al., 2023).

The Old Krakatau samples yielded the lowest pressure estimates of all the eruptive periods. Sample SERT1 yielded a pressure of 14–72 MPa, which corresponds to shallow magma storage at depths of 0.6–2.9 km. We tried to perform orthopyroxene-liquid thermobarometry on sample PJ3 but it was out of equilibrium, probably due to the abundance of silica minerals in the groundmass (Supplementary Figure S3A). Therefore, we plotted the total titanomagnetite Al_2O_3 and MgO contents against X_{Usp} (Figure 10B) to give a rough estimate of the crystallization pressure of PJ3. An experimental study by Mollo et al. (2013) showed that titanomagnetite formed at higher pressure (or deeper in volcanic systems) has higher Al_2O_3 + MgO contents and slightly lower Ti content than those formed at lower pressure. At higher pressures, Al_2O_3 and MgO in the melt are preferentially incorporated into crystals (Mollo et al., 2013). This is in line with the findings of Buddington and Lindsley

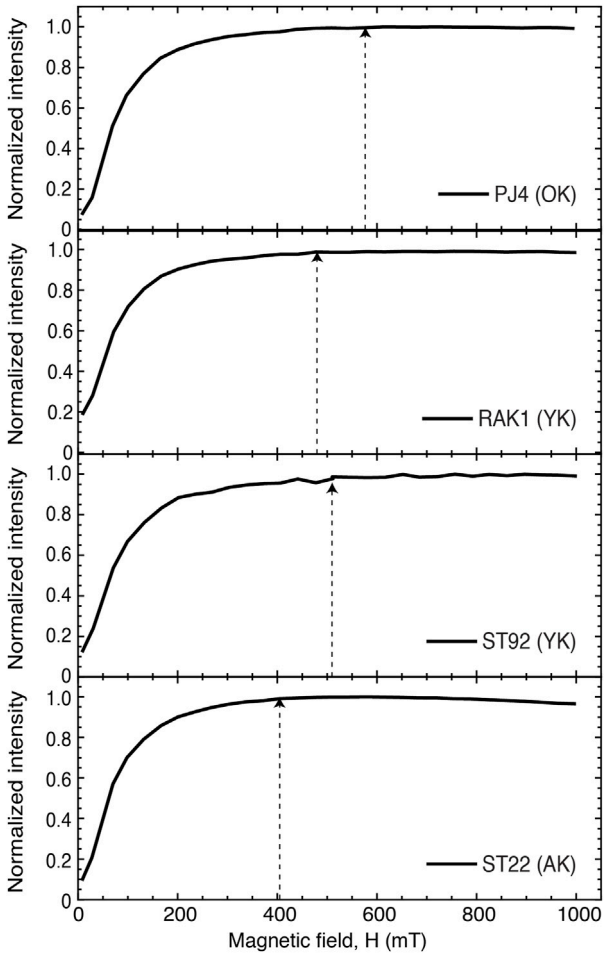

FIGURE 9
IRM acquisition curves of representative samples from each eruptive stage of Krakatau volcano. The vertical dashed lines indicate the average saturation magnetic field for each sample. OK = Old Krakakatu, YK = Young Krakatau, AK = Anak Krakatau.

(1964) and Anai et al. (2023), who show that, at low temperatures and pressures, titanomagnetite will be richer in Ti.

Figure 10B shows that titanomagnetite crystals in sample PJ3 have the lowest Al_2O_3 + MgO contents, which suggests shallow magma storage. Some of the titanomagnetite crystals from sample SERT1 yield similar but higher ranges of Al_2O_3 and MgO contents than those of PJ3, suggesting that SERT1 was stored at similar or deeper depths than PJ3. Overall, the titanomagnetite in PJ3 and SERT1 yields lower Al_2O_3 + MgO (Figure 10B) and higher TiO_2 (Figure 5B) contents than the Young and Anak Krakatau samples, suggesting that a shallow magma chamber was the source of the PJ3 (KTL1) and SERT1 (KTL2) lavas during the Old Krakatau period. However, given that our orthopyroxene-liquid thermobarometry yields a low pressure estimate for SERT1, which has a highly evolved whole-rock composition, we suggest that this pressure represents late-stage storage conditions.

The co-existence and compositions of titanomagnetite and ilmenite in the Old Krakatau samples, unlike in the Anak Krakatau samples which contain only titanomagnetite, could reflect different intensive parameters, in particular the oxygen fugacity (fO_2). However, estimating the oxygen fugacity of our samples is outside the scope of this study. The presence of ilmenite in the Old Krakatau samples, both as individual grains and as exsolution lamellae, could reflect more oxidized magma. According to Lanza and Meloni (2006), on the ternary Fe-Ti-O diagram (Figure 5A), Fe^{2+} ions plot on the left, while Fe^{3+} ions plot on the right, which implies that the degree of oxidation increases from left to right (from the titanomagnetite to titanohematite series). On the other hand, we observed composite or granule-like (Figure 7A) and trellis-like ilmenite exsolution (Figure 7B) within titanomagnetite hosts. These exsolution textures could be caused by oxidation of titanomagnetite minerals (Haggerty, 1991; Liao et al., 2016).

The presence of Ti-rich titanomagnetite and ilmenite in the Old Krakatau samples is supported by the low magnetic susceptibility. The Old Krakatau samples have lower magnetic susceptibilities than the Anak and Young Krakatau lava samples. High Ti contents of titanomagnetite weakens magnetic interaction forces between electrons, which lowers its magnetic properties (Lanza and Meloni, 2006). Ilmenite tends to be included as canted-antiferromagnetic and antiferromagnetic (Banerjee, 1991; Lanza and Meloni, 2006), leading to weak magnetic moments. Therefore, the presence of predominantly Ti-rich titanomagnetite as well as ilmenite decreases the magnetic susceptibility of the Old Krakatau samples. In addition, the lower magnetic susceptibilities of the Old Krakatau samples are consistent with their magnetic saturation fields, which are higher than those of the Anak Krakatau and Young Krakatau samples (Figure 8, Supplementary Table S6). The higher saturation field results from the presence of heterogeneous magnetic minerals in the Old Krakatau samples (both titanomagnetite and ilmenite). In particular, minerals in the titanohematite series (e.g., ilmenite, hematite), which have high coercivity values, raise magnetic saturation fields (Liebke et al., 2011; Kanamaru et al., 2022), even up to almost 1 T, as shown by Liebke et al. (2011).

6.1.2 Young Krakatau

The whole-rock compositions of the Young Krakatau products, including the 1883 pumice samples from Mandaville et al. (1996) and Madden-Nadeau et al. (2021), have a wide range of SiO_2 contents (Figure 3), from andesite to rhyodacite. The matrix-glass compositions of the Young Krakatau products are generally less evolved than those of the Old Krakatau products. It should be emphasized that despite being from the same period, the compositions of the Young Krakatau products on Harker diagrams (Supplementary Figure S4) show different trends. Compared to the Old Krakatau samples (particularly KTL1), the Young Krakatau products generally have 1) lower clino- and orthopyroxene FeO/MgO ratios and 2) lower titanomagnetite MnO/Al_2O_3 ratios with intermediate titanomagnetite Mg numbers (Figure 10A). The higher Mg numbers and lower titanomagnetite MnO/Al_2O_3 ratios of the Young Krakatau samples relative to the Old Krakatau samples suggest that they were produced from less differentiated magmas.

Magma storage during the Young Krakatau period, estimated using orthopyroxene-liquid thermobarometry, was deeper (1.1–3.4 km) than that of the Old Krakatau magmas. However, these depth estimates may not represent the whole storage region, as

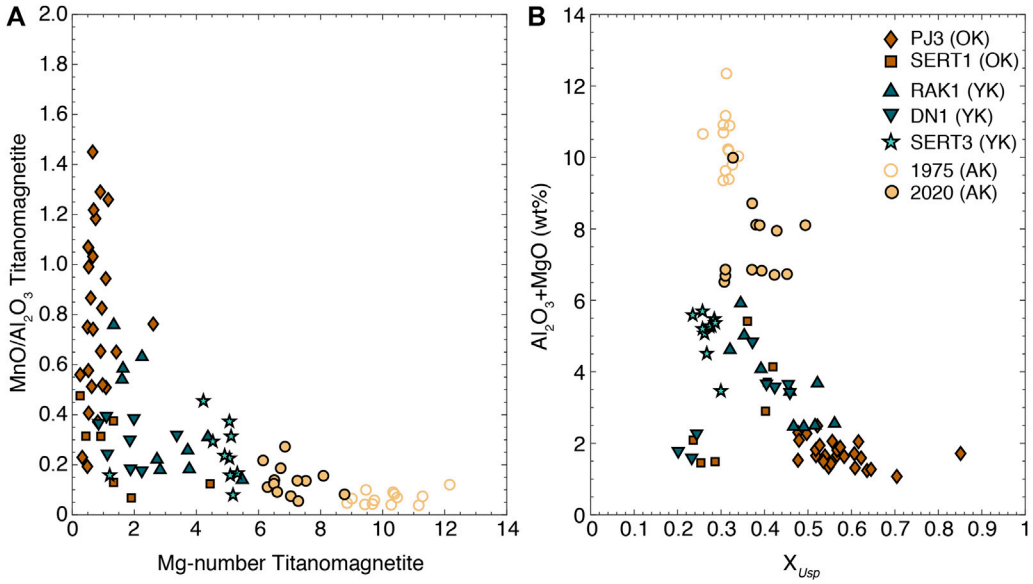

FIGURE 10
(A) The titanomagnetite MnO/Al_2O_3 ratios against Mg number. **(B)** Total Al_2O_3 and MgO contents of titanomagnetite as a function of ulvöspinel molar fractions (X_{Usp}). X_{Usp} is calculated following the method of Stormer (1983). OK = Old Krakakatu, YK = Young Krakatau, AK = Anak Krakatau.

the orthopyroxene yields low Al contents, which fits the model of Putirka (2008) for the crystallization of orthopyroxene from felsic magma or at low pressures. Our depth estimates differ from those of two previous studies. Mandeville et al. (1996) suggested that the top of the magma chamber was at 100–150 MPa (4–6 km), estimated from plagioclase-liquid equilibria using natural multi-component systems from experimental data of Housh and Luhr (1991). A recent study by Madden-Nadeau et al. (2021) reports pressures from R-MELTS modeling of 125–250 MPa (5–10 km) for Young Krakatau pumices. The difference between our results and those of previous studies is due to the different methods used; however, we do not think that the R-MELTS model is appropriate for Krakatau products because this magma does not contain quartz phenocrysts (e.g., Gualda and Ghiorso, 2014; Wilson et al., 2021).

In addition, the estimated crystallization depths of the Young Krakatau samples in this study are consistent with most of the Young Krakatau titanomagnetite, which have higher Al_2O_3 + MgO and lower Ti contents than those from Old Krakatau (Figures 10B, 5B), suggesting the titanomagnetite in Young Krakatau formed at higher pressure than that in Old Krakatau. At these depths, it appears that the Young Krakatau magmas have similar or lower degrees of oxidation than the Old Krakatau magmas, as the compositions of some of the Young Krakatau Fe-Ti oxides overlap with those from Old Krakatau (Figure 5A). In addition, the ilmenite exsolution lamellae and individual grains are found in the Young Krakatau samples (Figures 7E, G, I), implying that the fO_2 of Old and Young Krakatau were similar. However, the ilmenite exsolution lamellae in the Old Krakatau samples (more than 50% of the host area, Figure 7B) are more abundant than that in Young Krakatau (about 22% of the host area, Figure 7E). This may indicate that the Old Krakatau magma was more oxidized than that of Young Krakatau (the fO_2 of Old Krakatau was higher than that of Young Krakatau). According to Buddington and Lindsley (1964), Lattard (1995), Silva et al. (2008), and Unganai et al. (2022), the amount of ilmenite exsolved in a titanomagnetite host increases as oxidation increases and as the temperature decreases. The most recent study on the Krakatau 1883 pumice obtained an average oxygen fugacity (fO_2) of NNO+0.76 with an average final pre-eruption equilibration temperature of 914°C from titanomagnetite-ilmenite pairs (Madden-Nadeau et al., 2021).

The magnetic susceptibility of the Young Krakatau lava samples is higher than that of the Old Krakatau lava samples. This is due to the higher Fe and lower Ti contents of the titanomagnetite in the Young Krakatau lava samples than that in Old Krakatau. This also lowered the magnetic saturation of the Young Krakatau lava relative to that of the Old Krakatau samples (Figure 8B). The Young Krakatau pumice samples have very low magnetic susceptibility despite containing higher Fe and lower Ti contents than Old Krakatau. Another factor causing this low magnetic susceptibility in the pumice samples is the low abundances (or finer grain sizes) of magnetic Fe-Ti oxides minerals. Low magnetic susceptibility values in pumice samples are common in other volcanoes and regions, e.g., the Meidob Volcanic Field, Sudan (MS $<200 \times 10^{-5}$ SI Unit, Paulick and Franz, 1997), the Pahae Julu Region, North Sumatra Province, Indonesia (MS of 85–183.1 $\times 10^{-8}$ m^3/kg, Siregar et al., 2022), and Asama Volcano, Japan (MS of 240–400 $\times 10^{-8}$ m^3/kg, Kanamaru et al., 2022).

6.1.3 Anak Krakatau

Despite being basaltic, the recent lava sample erupted in 2020 has evolved matrix-glass compositions, reaching trachydacite (Figure 3), although the matrix glass is less evolved than those of representative Young and Old Krakatau samples (Figure 3). Compared to Old and Young Krakatau samples, the Anak Krakatau products generally have 1) the lowest clino- and orthopyroxene FeO/MgO ratios and 2) the lowest titanomagnetite MnO/Al_2O_3 with the highest titanomagnetite Mg numbers

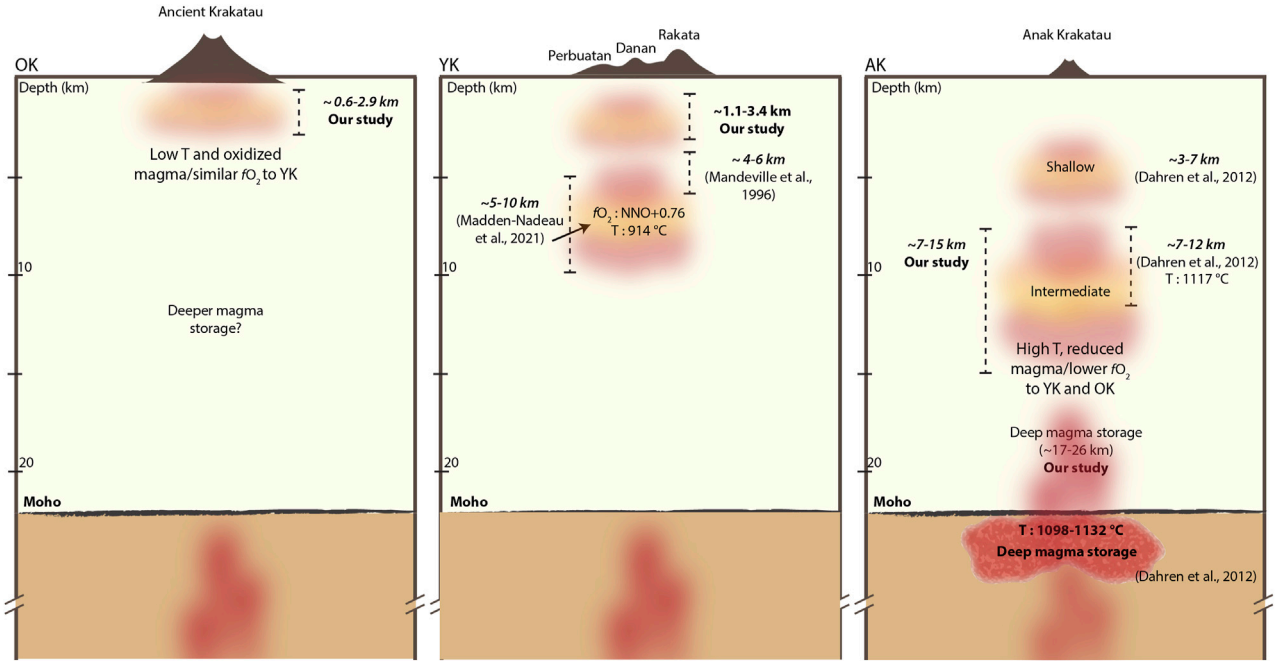

FIGURE 11
Illustration of the magma storage conditions during the three eruptive periods: Old Krakatau, Young Krakatau, and Anak Krakatau. The Moho depth is from Harjono et al. (1989). Horizontal view is not to scale.

(Figure 10A). This suggests that the Anak Krakatau lavas were much less differentiated than the Young and Old Krakatau magmas.

Two-pyroxene pressure estimates indicate that the recent 2020 Anak Krakatau lava originated from intermediate to deep storage areas, with small and large pyroxene pairs yielding depths of 7.4–15.6 km and >17 km, respectively. This is consistent with the high MnO/Al_2O_3 ratios and low Ti contents of titanomagnetite from the Anak Krakatau samples (Figures 10B, 5B), indicating crystallization at higher pressures (Mollo et al., 2013) than the Young and Old Krakatau samples. In addition, our estimates of the magma storage depth are well correlated to the intermediate (7–12 km) and deep (>22 km) storage regions of Dahren et al. (2012). In contrast to the Old and Young Krakatau samples, the only magnetic mineral in the Anak Krakatau samples is titanomagnetite, and ilmenite is present only as exsolution lamellae comprising less than 10% of host volume (Figure 7L). The abundance of titanomagnetite in the Anak Krakatau samples leads to the highest magnetic susceptibility and lowest magnetic saturation of all samples. In addition, titanomagnetite is characterized by low coercivity, so that saturation occurs at low magnetic fields (Liebke et al., 2011).

The results above suggest that the Anak Krakatau samples were less oxidized than the Old and Young Krakatau samples. This is also supported by the low amount of ilmenite exsolution lamellae (Figure 7L) that formed by direct exsolution at low fO_2 and high temperatures (Tan et al., 2016). In addition, Dahren et al. (2012) estimated average magma storage temperatures at intermediate crustal depths beneath Anak Krakatau of 1,117°C using clinopyroxene-melt thermobarometry on 1990–2002 AK eruptive products. An older, 1963 basalt from Anak Krakatau also yielded average magma storage temperatures of 1,098°C (with 3 wt% H_2O) and 1,132°C (with 2 wt% H_2O), estimated using plagioclase-melt thermobarometry at depths of 23 km and 29 km, respectively (Dahren et al., 2012). The temperatures of Anak Krakatau magmas are generally >1,000°C, higher than that of Young Krakatau, as also reported by Agangi and Reddy (2016) for 2008 eruptive products.

In summary, we present a simple model of the plumbing system of each period of Krakatau in Figure 11. It should be noted that the studied samples do not cover the full range of units within each period (see Table 1), particularly the Old and Young Krakatau periods. However, the distinct feature of our studied samples, particularly the lava samples, is that the whole-rock compositions trend towards less silicic compositions from Old to Anak Krakatau, and the magma storage depths estimated from the crystallizing depths of the minerals in representative samples get deeper. This does not exclude the possibility of the other storage regions, which could be revealed by samples we have not yet collected, but we suggest that for a certain time during each period corresponding to the lava samples, magmatic activity was pronounced in those regions.

6.2 The eruptive cycle of Krakatau

Krakatau has experienced phases of growth and collapse of its edifice throughout its eruptive history (Francis, 1985; Bronto, 2000; Sutawidjaja, 2006). The collapse events were associated with caldera-forming eruptions (CFE) in 1883 and presumably 416 AD, as well as volcanogenic tsunamis (e.g., in 1883 and 2018). After the first CFE, eruptive activity resumed through the growth of Rakata island and subsequent formation of the new Danan and Perbuatan cones

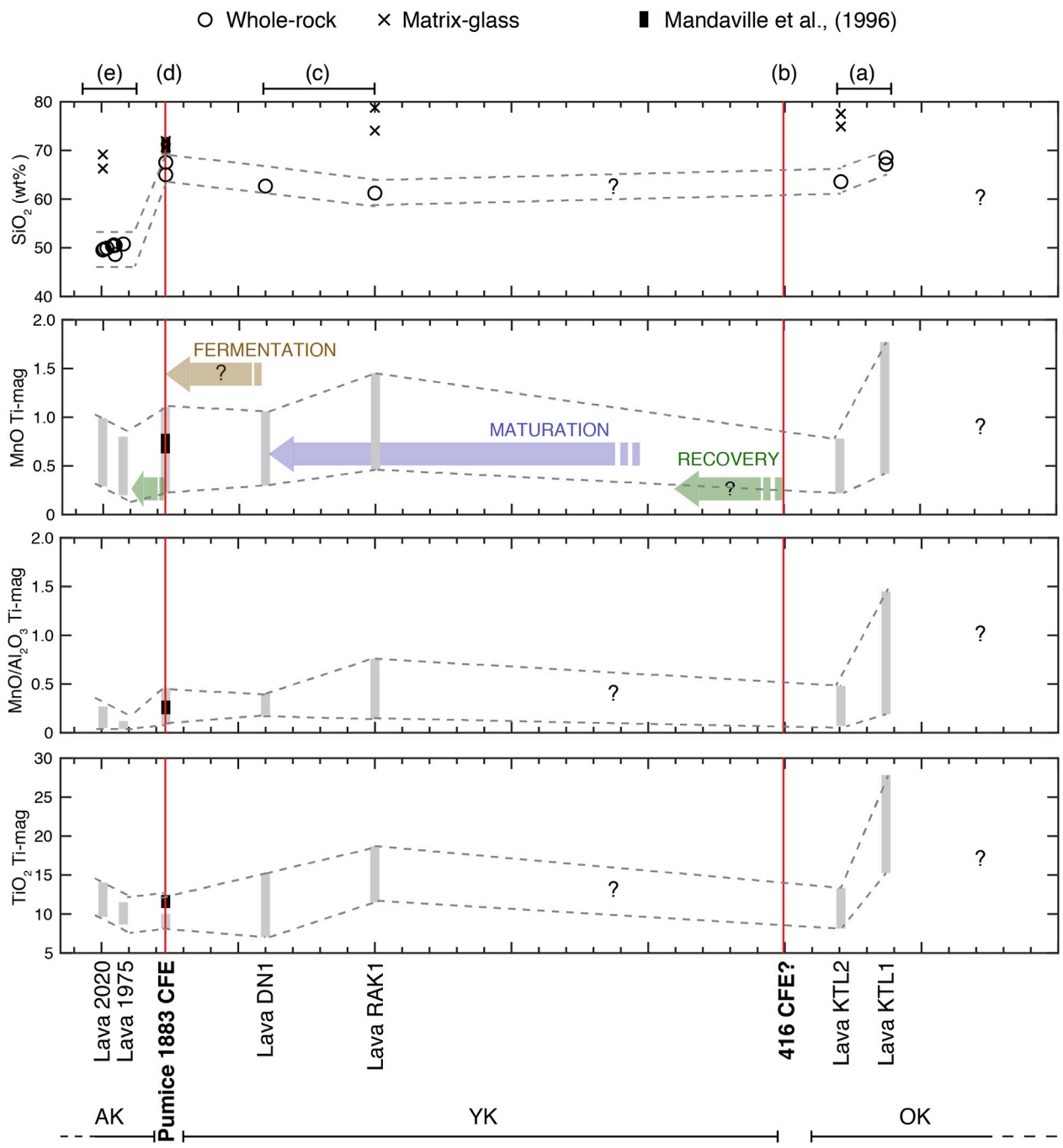

FIGURE 12
Whole-rock SiO_2 contents of all samples and matrix-glass SiO_2 contents of representative samples, as well as titanomagnetite MnO contents and MnO/Al_2O_3 ratios of Old Krakatau (OK), Young Krakatau (YK), and Anak Krakatau (AK) lava samples, including YK pumice from the second CFE in 1883. The TiO_2 content of titanomagnetite is also plotted, as it shows clear changes across the samples. The visualization of the diagram follows Bouvet de Maisonneuve et al. (2021).

(Francis, 1985). This growth was then destroyed by the second CFE in 1883, which was followed by the growth of Anak Krakatau. Due to this cyclic activity involving CFEs, Krakatau can be classified as a polycyclic system, i.e., having formed more than one caldera (Bouvet de Maisonneuve et al., 2021). We focus our discussion on the chemical evolution of the melts and minerals (particularly titanomagnetite) in this cyclic system, excluding what triggered the Krakatau CFEs. Readers can refer to Madden and Nadeau et al. (2021) for the eruption mechanism of the 1883 CFE.

Stratigraphically, we suggest that our Old Krakatau samples preceded the first CFE (416 AD), with that CFE defining the end of the Old Krakatau period. The Young Krakatau lava samples were erupted before the second CFE in 1883 and belong to the Rakata and Danan series. The Young

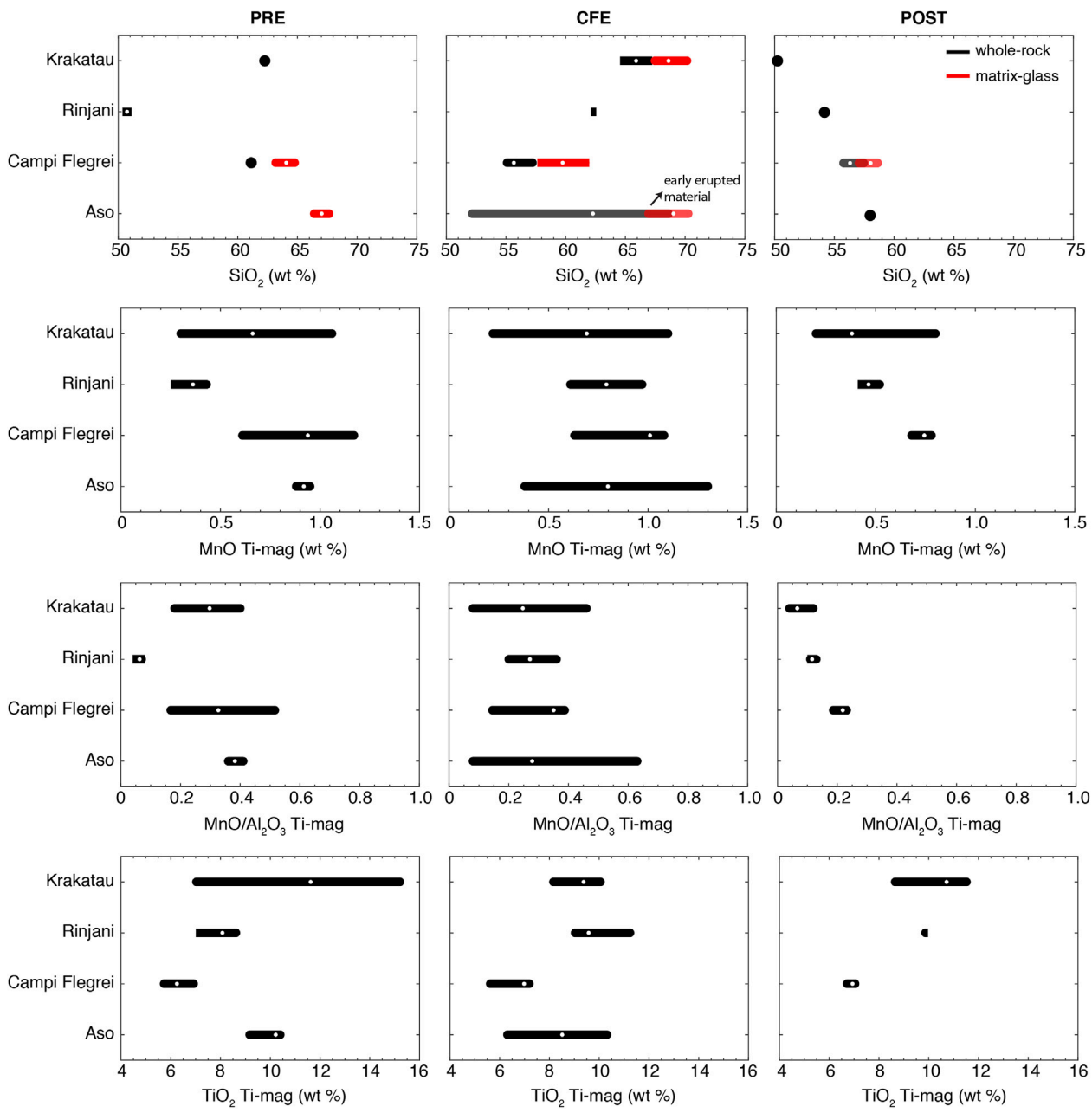

FIGURE 13
The comparison of pre-, syn-, and post-caldera forming eruption (CFE) in the chemical contents of SiO_2 of whole-rock and matrix-glass and of MnO, ratio of MnO/Al_2O_3, and TiO_2 of titanomagnetite. The pre- and post-CFE are taken for the closer and available event/data prior to and after, respectively. Pre: Krakatau-Danan lava, Rinjani-PcSF4 scoria, Campi Flegrei-Verdolino pumice, and Aso-Aso A pumice. Syn: Krakatau-1883 pumice, Rinjani-1257 pumice, Campi Flegrei-Neapolitan Yellow Tuff pumice, and Aso-Aso 4 pumice. Post: Anak Krakatau-1975 lava, Rinjani-Barujari 2004 lava, Campi Flegrei-Pomici Principali pumice, and Aso-Yamasaki Pumice 10. The white dots indicate an average of data. Data is from this study for Krakatau, Vidal et al. (2015) and Métrich et al. (2018) for Rinjani, Forni et al. (2016, Forni et al., 2018) and references therein for Campi Flegrei, Miyabuchi (2009) and Keller et al. (2021), Keller et al. (2023) for Aso.

Krakatau pumice samples are products of the second CFE, which defined the end of the Young Krakatau period. Figure 12, adapted from Bouvet de Maisonneuve et al. (2021), shows the whole-rock and matrix-glass silica contents and the MnO, MnO/Al_2O_3, and TiO_2 contents of titanomagnetite crystals from our samples, which cover more than one caldera cycle. In one caldera cycle, there are three stages: pre-collapse activity, the caldera-forming eruption, and post-collapse activity. Detailed characteristics of each stage can be seen in Table 1 of Bouvet de Maisonneuve et al. (2021).

In Figure 12, stages *a* and *c* have similar whole-rock and matrix-glass compositions and titanomagnetite MnO contents and MnO/Al_2O_3 ratios. The liquid compositions are more evolved and the corresponding samples, the Old and Young Krakatau lava samples, have relatively high titanomagnetite MnO contents and MnO/Al_2O_3 ratios, implying that they were the most differentiated. In addition,

magma was stored during these stages in shallow regions (Figure 11). These geochemical characteristics are indicative of the maturation phase or perhaps the beginning of the fermentation phase. For instance, Rabaul Caldera is currently in a mid-maturation phase, indicated by high SiO_2 contents (dacitic magma). In addition, the crystallization pressures estimated for the products of the August 2014 eruption are low (<100 MPa; Fabbro et al., 2020) indicating shallow magma storage. This is similar to the maturation phase of the Old and Young Krakatau lava samples, which record shallow magma storage (14–84 MPa).

Stages *b* and *d* were CFEs. It appears that the titanomagnetite MnO contents and MnO/Al_2O_3 ratios during the maturation phase (particularly shown by lava sample RAK1) are higher than those in the 1883 CFE event itself. This trend is clear at Rabaul Caldera, preceding the Rabaul Pyroclastics caldera collapse (1400 BP), and also observed at Campi Flegrei preceding the Neapolitan Yellow Tuff (~14.9 ka) (Bouvet de Maisonneuve et al., 2021).

During the maturation phase, smaller magma reservoirs can grow and coalesce, forming larger, interconnected magma reservoirs at shallow depths. This will lead to an increase in the volume of silicic magma and volatile contents from continuing crystallization while the flux of mafic magma from the lower crust wanes (Degruyter and Huber, 2014; Pansino and Taisne, 2019; Bouvet de Maisonneuve et al., 2021). The geometry of this large shallow magma reservoir will change after a CFE due to the collapse of the roof of that reservoir (Bouvet de Maisonneuve et al., 2021).

Stage *e* in Figure 12 is the incubation phase, after the 1883 CFE, indicated by the mafic compositions of the Anak Krakatau products (Figure 3), which are less differentiated than the Young Krakatau and Old Krakatau magmas based on their lower titanomagnetite MnO/Al_2O_3 ratios, but generally hotter than the Young and Old Krakatau magmas. In addition, this phase is also indicated by frequent but small eruptions (Bouvet de Maisonneuve et al., 2021), as has been observed to date. Instead of a waning caldera cycle, Krakatau repeated the cycle after the two CFEs by growing and forming new cones, including Rakata, Danan, Perbuatan, and Anak Krakatau, with Anak Krakatau emerging from the sea in 1927. In addition, Abdurrachman et al. (2018) suggested that there is mantle upwelling beneath Anak Krakatau supplying new magma batches to the upper magma reservoir(s). As Krakatau has undergone two CFEs, it has potential to occur in the future, when the mafic magmas of the Anak Krakatau period continue differentiating and become more evolved: one of the characteristics of a system heading towards a CFE.

6.3 The comparison of Krakatau with several calderas around the world

We compared the evolution of Krakatau with other calderas, i.e., Rinjani in Indonesia, Campi Flegrei in Italy, and Aso in Japan, in terms of the chemical changes from pre-, syn-, and post-CFE; regardless the time lapse from the previous event to the CFE and from CFE to post event as well as the composition and type of eruptive product. Since some of the volcanoes have experienced more than one caldera-forming eruption (i.e., Krakatau, Campi Flegrei, Aso), we take the last CFE event of each volcano for the comparison.

Krakatau and Rinjani have a similar trend of increasing SiO_2 content of whole-rock towards the CFE and decreased afterwards (Figure 13). The increase in SiO_2 in Krakatau and Rinjani from pre-to the CFE event could be resulted from an intense magma differentiation (e.g., Bouvet de Maisonneuve et al., 2021). Meanwhile, the decreased SiO_2 content of whole-rock post-CFE is due to an injection of basaltic magma, which feeds Anak Krakatau and Barujari (Dahren et al., 2012; Métrich et al., 2017). Similarly, Aso displays increasing SiO_2 content of matrix-glass towards CFE and decreasing SiO_2 content of whole-rock after CFE. On the contrary, Campi Flegrei shows decreasing SiO_2 content of whole-rock and matrix-glass towards the CFE, but these values, respectively, remain similar and continue to decrease after CFE. The decrease in SiO_2 content of magma in Campi Flegrei may be related to the continuous injections from deeper magma reservoirs (Pabst et al., 2008; Forni et al., 2018).

Krakatau, Rinjani, and Campi Flegrei display a similar trend of MnO and MnO/Al_2O_3 content titanomagnetite where it generally decreases after the CFE. The MnO content and ratio of MnO/Al_2O_3 titanomagnetite for Aso seems to increase during the CFE. As mentioned in the previous Section 5.2, higher MnO and MnO/Al_2O_3 ratio of titanomagnetite indicate higher degrees of differentiation and *vice versa*. The lower degree of magma differentiation is accompanied by the injection of less evolved magma. Lastly, the TiO_2 contents of titanomagnetite in the pre-, syn-, and post-CFE samples do not offer a unique signature, meaning that each volcano shows different trends.

7 Conclusion

We analyzed samples representing three periods at Krakatau, Old Krakatau, Young Krakatau, and the most recent, Anak Krakatau, to improve our understanding of magma evolution at Krakatau. This study shows that a complex magma plumbing system has persisted along the evolution of the Krakatau edifice. The melt and mineral (pyroxene and Fe-Ti oxides) chemistry and the magnetic properties of the rock samples varies within each period. The magnetic properties of the rocks are consistent with the type, abundance, and composition of the Fe-Ti oxides (titanomagnetite and ilmenite were present in our samples). Those samples with titanomagnetite as the only Fe-Ti oxide, i.e., the Anak Krakatau samples, have high magnetic susceptibility values, whereas, this value decreased when ilmenite was present, as observed in the Old and Young Krakatau samples.

This work and previous studies show that the erupted magma came from various depths and different melt reservoirs, indicating that there is progressive or repeated accumulation of magma feeding the Krakatau systems. The crystallization pressures estimated from the studied samples indicate shallow magma storage during the Old and Young Krakatau periods (0.6–3.4 km), while Anak Krakatau magma storage ranged from intermediate depths to depths of up to 26 km. In the shallow reservoirs, the Old and Young Krakatau magmas were more differentiated, but the Old Krakatau magmas may have been more oxidized and colder than the Young Krakatau

magmas. The deeper magmas of AK were less differentiated and may have been less oxidized than the Young and Old Krakatau magmas but were hotter.

We also placed our samples in the corresponding stages of the caldera cycle. Krakatau is a polycyclic caldera system, as it has experienced multiple caldera-forming eruptions. The Old and Young Krakatau lava samples erupted during the maturation phase that continued to generate the first and second caldera-forming eruptions, respectively. The second caldera forming-eruption produced the Young Krakatau pumice samples and was followed by the formation of Anak Krakatau, which is currently in the incubation phase. Thus, understanding the characteristics of each stage in the caldera cycle will contribute to interpreting the conditions at which feeding magmas are stored, and hence, a time-series of changes that the magmatic plumbing system experiences.

In comparison with other caldera systems, advanced magma differentiation appeared to be the dominant process preceding the CFE of Krakatau 1883, Rinjani 1,257, and Aso 4, characterized by an increased SiO_2 content of matrix-glass, as well as MnO and MnO/Al_2O_3 ratio of titanomagnetite. However, Campi Flegrei (NYT) shows the opposite chemical signatures, as the system underwent an active injection of less evolved magma prior to the CFE. However, it should be emphasized that this study used limited samples from the Old, Young, and Anak Krakatau periods. Therefore, further research with a larger number and variety of samples is required to provide a more complete insight into the evolution of Krakatau.

Data availability statement

The original contributions presented in the study are included in the article/Supplementary Material, further inquiries can be directed to the corresponding authors.

Author contributions

AP and DN contributed as the main contributors of this paper. AP, DN, PS, MA, SB, and EK contributed to conception and design of the study. AP, DN, PS, TI, WB, MA, and IK collected the samples in the field. AP, DN, PS conceived and designed the experiments. PS and NA performed rock magnetic measurements. AP, PS, DN, TI, and RN performed SEM-EDS analysis. DN, GB, and NS performed EPMA analysis. AP, PS, MH, SB, and NA analyzed the rock magnetic data. AP and RN analyzed the magnetic minerals chemistry and textural data. DN, GB, MA, IK, and NS analyzed the non-magnetic minerals chemistry and textural data. AP, PS, and DN wrote the first draft of the manuscript. All authors contributed to manuscript revision, read, and approved the submitted version.

Funding

This study was financially supported by the Earth Science and Maritime Research Organization, National Research and Innovation Agency of the Republic of Indonesia through Rumah Program Kebencanaan (Nos. SP DIPA-124.01.1.690501/2022 and SP DIPA-124.01.1.690501/2023) grant to AP, EK, DN, MA, SB, and NA. Additional funding was also received from Faculty of Earth Sciences and Technology, Bandung Institute of Technology through Post-Doctoral Research Grants to AP (Nos. 1607A/IT1.C01/KS.00/2022 and 2779D/IT1.C01/KP-KS.00/2023) and was also supported by the Post-Doctoral Research Grants from National Research and Innovation Agency Republic of Indonesia (BRIN) to DN (No. 64/II/HK/2022) and GB (No. 15/II/HK/2023).

Acknowledgments

Permission to conduct field research at Krakatau volcano was given by the BKSDA (Balai Konservasi Sumber Daya Alam or Natural Resource Conservation Center) of Bengkulu-Lampung, Indonesia. Our thanks also go to Muhammad Zain Tuakia, Windi Anarta Draniswari, Cinantya Nirmala Dewi, and Mohammad Hasib for the fruitful discussion and their assistance with the laboratory work. We are grateful to Petrography Laboratory of Balai Penyelidikan dan Pengembangan Teknologi Kebencanaan Geologi (BPPTKG), CVGHM, Geological Agency of Indonesia, for helping us making thin sections, Tri Rahmawati for her assistance during the EPMA analysis and Gareth Fabbro for English language editing.

Conflict of interest

The authors declare that the research was conducted in the absence of any commercial or financial relationships that could be construed as a potential conflict of interest.

Publisher's note

Supplementary material

The Supplementary Material for this article can be found online at: https://www.frontiersin.org/articles/10.3389/feart.2023.1128798/full#supplementary-material

References

Abdurrachman, M., Widiyantoro, S., Priadi, B., and Ismail, T. (2018). Geochemistry and structure of krakatoa volcano in the sunda strait, Indonesia. *Geosci* 8, 111. doi:10.3390/geosciences8040111

Agangi, A., and Reddy, S. M. (2016). Open-system behaviour of magmatic fluid phase and transport of copper in arc magmas at Krakatau and Batur volcanoes, Indonesia. *J. Volcanol. Geoth. Res.* 327, 669–686. doi:10.1016/j.jvolgeores.2016.10.006

Amor, K., Hesselbo, S. P., Porcelli, D., Price, A., Saunders, N., Sykes, M., et al. (2019). The mesoproterozoic stac fada proximal ejecta blanket, NW scotland: constraints on crater location from field observations, anisotropy of magnetic susceptibility, petrography, and geochemistry. *J. Geol. Soc. Lond.* 176, 830–846. doi:10.1144/jgs2018-093

Anai, C., Ohkura, T., Yoshikawa, S., and Mochizuki, N. (2023). Temporal change in rock-magnetic properties of volcanic ashes ejected during a 1-year eruption event: A case study on the Aso nakadake 2019–2020 eruption. *Earth, Planets Space* 75 (1), 24. doi:10.1186/s40623-023-01783-x

Banerjee, S. K. (1991). Magnetic properties of Fe-Ti oxides. *Rev. Mineral. Geochem.* 25 (1), 107–128. doi:10.1515/9781501508684-007

Bouvet De Maisonneuve, C., Forni, F., and Bachmann, O. (2021). Magma reservoir evolution during the build up to and recovery from caldera-forming eruptions – generalizable model? *Earth Sci. Rev.* 218, 103684. doi:10.1016/j.earscirev.2021.103684

Bronto, S. (2000). Volcanic hazard assessment of Krakatau Volcano, sunda strait Indonesia. *Bull. Environ. Geol.* 12, 20–29.

Buddington, A. F., and Lindsley, D. H. (1964). Iron-Titanium oxide minerals and synthetic equivalents. *J. Petrol.* 5 (2), 310–357. doi:10.1093/petrology/5.2.310

Camus, G., Gourgaurd, A., and Vincent, P. M. (1987). Petrologic evolution of Krakatau (Indonesia): implications for a future activity. *J. Volcanol. Geoth. Res.* 33, 299–316. doi:10.1016/0377-0273(87)90020-5

Cañón-Tapia, E., and Pinkerton, H. (2000). The anisotropy of magnetic susceptibility of lava flows: an experimental approach. *J. Volcanol. Geoth. Res.* 98, 219–233. doi:10.1016/s0377-0273(99)00155-9

Chi, C., and Dorobek, S. (2004). Cretaceous palaeomagnetism of indochina and surrounding regions: cenozoic tectonic implications. *J. Geol. Soc. Lond.* 226, 273–287. doi:10.1144/GSL.SP.2004.226.01.15

Cinku, M. C., Rammlmair, D., Hisarli, M. H., and Orbay, N. (2009). A combined rock magnetic and geochemical investigation of upper cretaceous volcanic rocks in the pontides, Turkey. *Stud. Geophys. Geod.* 53, 475–494. doi:10.1007/s11200-009-0035-5

Cutler, K. S., Watt, S. F. L., Cassidy, M., Madden-Nadeau, A. L., Engwell, S. L., Abdurrachman, M., et al. (2022). Downward-propagating eruption following vent unloading implies no direct magmatic trigger for the 2018 lateral collapse of Anak Krakatau. *Earth Planet. Sc. Lett.* 578, 117332. doi:10.1016/j.epsl.2021.117332

Dahren, B., Troll, V. R., Anderson, U. B., Chadwick, J. P., Gardner, M. F., Jaxybulatov, K., et al. (2012). Magma plumbing beneath Anak Krakatau volcano, Indonesia: evidence for multiple magma storage regions. *Contrib. Mineral. Petrol.* 163, 631–651. doi:10.1007/s00410-011-0690-8

Degruyter, W., and Huber, C. (2014). A model for eruption frequency of upper crustal silicic magma chambers. *Earth Planet. Sci. Lett.* 403, 117–130. doi:10.1016/j.epsl.2014.06.047

Effendi, A. C., Sukhyar, R., and Bronto, S. (1983). *Geology of Krakatau complex, symposium 100 years Krakatau 1883-1983*. Jakarta: VSI Bandung, 1–17. 23-27 August 1983.

Fabbro, G. N., McKee, C. O., Sindang, M. E., Eggins, S., and Bouvet De Maisonneuve, C. (2020). Variable mafic recharge across a caldera cycle at Rabaul, Papua New Guinea. *J. Volcanol. Geotherm.* 393, 106810. doi:10.1016/j.jvolgeores.2020.106810

Ferré, E. C., Geissman, J. W., and Zechmeister, M. S. (2012). Magnetic properties of fault pseudotachylytes in granites: magnetic properties of pseudotachylytes. *J. Geophys. Res.* 117, B01106. doi:10.1029/2011JB008762

Forni, F., Bachmann, O., Mollo, S., De Astis, G., Gelman, S. E., and Ellis, B. S. (2016). The origin of a zoned ignimbrite: insights into the campanian ignimbrite magma chamber (Campi Flegrei, Italy). *Earth Planet. Sci. Lett.* 449, 259–271. doi:10.1016/j.epsl.2016.06.003

Forni, F., Degruyter, W., Bachmann, O., De Astis, G., and Mollo, S. (2018). Long-term magmatic evolution reveals the beginning of a new caldera cycle at Campi Flegrei. *Sci. Adv.* 4 (11), eaat9401. doi:10.1126/sciadv.aat9401

Francis, P. W. (1985). The origin of the 1883 Krakatau tsunamis. *J. Volcanol. Geoth. Res.* 25 (3), 349–363. doi:10.1016/0377-0273(85)90021-6

Gardner, M. F., Troll, V. R., Gamble, J. A., Gertisser, R., Hart, G. L., Ellam, R. M., et al. (2013). Crustal differentiation processes at Krakatau Volcano, Indonesia. *J. Petrol.* 54, 149–182. doi:10.1093/petrology/egs066

Grilli, S. T., Zhang, C., Kirby, J. T., Grilli, A. R., Tappin, D. R., Watt, S. F. L., et al. (2021). Modeling of the dec. 22nd 2018 Anak Krakatau volcano lateral collapse and tsunami based on recent field surveys: comparison with observed tsunami impact. *Mar. Geol.* 440, 106566. doi:10.1016/j.margeo.2021.106566

Gualda, G. A., and Ghiorso, M. S. (2014). Phase-equilibrium geobarometers for silicic rocks based on rhyolite-MELTS. Part 1: principles, procedures, and evaluation of the method. *Contrib. to Mineral. Petrol.* 168 (1033), 1–17. doi:10.1007/s00410-014-1033-3

Haag, M. B., de Freitas, R. B., Sommer, C. A., Savian, J. F., Lima, E. F., Gambeta, J. H., et al. (2021). Multi-proxy case study of a neoproterozoic rhyolite flow in southernmost Brazil: emplacement mechanisms and implications for ancient felsic lavas. *J. S. Am. Earth Sci.* 107, 102982. doi:10.1016/j.jsames.2020.102982

Haggerty, S. E. (1991). Oxide textures: a mini atlas. *Rev. Mineral. Geochem* 25 (1), 129–219. doi:10.1515/9781501508684-008

Harjono, H., Diament, M., Nouaili, L., and Dubois, J. (1989). Detection of magma bodies beneath Krakatau volcano (Indonesia) from anomalous shear waves. *J. Volcanol. Geoth. Res.* 39 (4), 335–348. doi:10.1016/0377-0273(89)90097-8

Housh, T. B., and Luhr, J. F. (1991). Plagioclase-melt equilibria in hydrous systems. *Am. Mineralogist* 76 (3-4), 477–492.

Hunt, J. E., Tappin, D. R., Watt, S. F. L., Susilohadi, S., Novellino, A., Ebmeier, S. K., et al. (2021). Submarine landslide megablocks show half of Anak Krakatau island failed on December 22nd, 2018. *Nat. Commun.* 12, 2827. doi:10.1038/s41467-021-22610-5

Ismail, T., Abdurrachman, M., Rizal, Y., and Hardjawidjaksana, K. (2020). Volcanostratigraphy of krakatoa islands, south lampung district, lampung Province. *IOP C. Ser. Earth Env.* 589, 012010. doi:10.1088/1755-1315/589/1/012010

Kanamaru, T., Furukawa, K., Zhao, X., and Suganuma, Y. (2022). Magnetic petrology of pumice fall deposits of the 1783 eruption of Asama volcano, Japan. *Earth Planets Space* 74, 53. doi:10.1186/s40623-022-01618-1

Keller, F., Bachmann, O., Geshi, N., and Miyakawa, A. (2021). The role of crystal accumulation and cumulate remobilization in the formation of large zoned ignimbrites: insights from the aso-4 caldera-forming eruption, kyushu, Japan. *Front. Earth Sci.* 8, 614267. doi:10.3389/feart.2020.614267

Keller, F., Guillong, M., Geshi, N., Miyakawa, A., and Bachmann, O. (2023). Tracking caldera cycles in the Aso magmatic system – Applications of magnetite composition as a proxy for differentiation. *J. Volcanol. Geotherm. Res.* 436, 1–12. doi:10.1016/j.jvolgeores.2023.107789

Lanza, R., and Meloni, A. (2006). *The earth's magnetism. An introduction for geologists*. New York: Springer-Verlag.

Lattard, D. (1995). Experimental evidence for the exsolution of ilmenite from titaniferous spinel. *Am. Min.* 80, 968–981. doi:10.2138/am-1995-9-1013

Le Bas, M. J., Le Maitre, R. W., Streckeisen, A., and Zanettin, B. (1986). A chemical classification of volcanic rocks based on the total alkali-silica diagram. *J. Petrol.* 27, 745–750. doi:10.1093/petrology/27.3.745

Lerner, G. A., Piispa, E. J., Bowles, J. A., and Ort, M. H. (2022). Paleomagnetism and rock magnetism as tools for volcanology. *B. Volcanol.* 84, 24. doi:10.1007/s00445-022-01529-9

Liao, M., Tao, Y., Song, X., Li, Y., and Xiong, F. (2016). Study of oxygen fugacity during magma evolution and ore genesis in the Hongge mafic–ultramafic intrusion, the Panxi region, SW China. *Acta Geochim.* 35, 25–42. doi:10.1007/s11631-015-0064-4

Liebke, U., Antolín-Tomas, B., Appel, E., Basavaiah, N., Mikes, T., Dunkl, I., et al. (2011). Indication for clockwise rotation in the Siang window south of the eastern Himalayan syntaxis and new geochronological constraints for the area. *J. Geol. Soc. Lond.* 353, 71–97. doi:10.1144/SP353.5

Madden-Nadeau, A. L., Cassidy, M., Pyle, D. M., Mather, T. A., Engwell, S. L., Watt, S. F. L., et al. (2021). The magmatic and eruptive evolution of the 1883 caldera-forming eruption of Krakatau: integrating field-to crystal-scale observations. *J. Volcanol. Geoth. Res.* 411, 107176. doi:10.1016/j.jvolgeores.2021.107176

Maeno, F., and Imamura, F. (2011). Tsunami generation by a rapid entrance of pyroclastic flow into the sea during the 1883 Krakatau eruption, Indonesia. *J. Geophys. Res.* 116, B09205. doi:10.1029/2011JB008253

Mandeville, C. W., Carey, S., and Sigurdsson, H. (1996). Magma mixing, fractional crystallization, and volatile degassing during the 1883 eruption of Krakatau volcano, Indonesia. *J. Volcanol. Geoth. Res.* 74, 243–274. doi:10.1016/S0377-0273(96)00060-1

Métrich, N., Vidal, C. M., Komorowski, J. C., Pratomo, I., Michel, A., Kartadinata, N., et al. (2017). New insights into magma differentiation and storage in holocene crustal reservoirs of the lesser sunda arc: the rinjani–samalas volcanic complex (lombok, Indonesia). *J. Petrology* 58 (11), 2257–2284. doi:10.1093/petrology/egy006

Miyabuchi, Y. (2009). A 90,000-year tephrostratigraphic framework of Aso Volcano, Japan. *Sediment. Geol.* 220 (3-4), 169–189. doi:10.1016/j.sedgeo.2009.04.018

Mollo, S., Putirka, K., Iezzi, G., and Scarlato, P. (2013). The control of cooling rate on titanomagnetite composition: implications for a geospeedometry model applicable to alkaline rocks from Mt. Etna volcano. *Contrib. Mineral. Petrol.* 165, 457–475. doi:10.1007/s00410-012-0817-6

Muhari, A., Heidarzadeh, M., Susmoro, H., Nugroho, H. D., Kriswati, E., Supartoyo, , et al. (2019). The december 2018 Anak Krakatau Volcano tsunami as inferred from post-tsunami field surveys and spectral analysis. *Pure Appl. Geophys.* 176, 5219–5233. doi:10.1007/s00024-019-02358-2

Mutaqin, B. W., Lavigne, F., Hadmoko, D. S., and Ngalawani, M. N. (2019). Volcanic eruption-induced tsunami in Indonesia: A review. *IOP C. Ser. Earth Env.* 256, 012023. doi:10.1088/1755-1315/256/1/012023

Nagata, T. (2013). "Identification of magnetic minerals in rocks using methods based on their magnetic properties," in *Methods in palaeomagnetism developments in solid Earth geophysics*. Editors D. W. Collinson, K. M. Creer, and S. K. Runcorn (Elsevier), 501–513. doi:10.1016/B978-1-4832-2894-5.50086-0

Novellino, A., Engwell, S. L., Grebby, S., Day, S., Cassidy, M., Madden-Nadeau, A. L., et al. (2020). Mapping recent shoreline changes spanning the lateral collapse of Anak Krakatau Volcano, Indonesia. *Appl. Sci.* 10, 536. doi:10.3390/app10020536

O'Reilly, W. (1984). *Rock and mineral magnetism*. Glasgow: Blackie and Son Limited.

Pabst, S., Wörner, G., Civetta, L., and Tesoro, R. (2008). Magma chamber evolution prior to the campanian ignimbrite and neapolitan Yellow Tuff eruptions (Campi Flegrei, Italy). *Bull. Volcanol.* 70, 961–976. doi:10.1007/s00445-007-0180-z

Pansino, S., and Taisne, B. (2019). How magmatic storage regions attract and repel propagating dikes. *J. Geophys. Res.* 124, 274–290. doi:10.1029/2018JB016311

Paulick, H., and Franz, G. (1997). The color of pumice: case study on a trachytic fall deposit, Meidob volcanic field, Sudan. *Bull. Volcanol.* 59, 171–185. doi:10.1007/s004450050184

Pratama, A., Bijaksana, S., Abdurrachman, M., and Santoso, N. (2018). Rock magnetic, petrography, and geochemistry studies of lava at the ijen volcanic complex (IVC), banyuwangi, east Java, Indonesia. *Geosci.* 8, 183. doi:10.3390/geosciences8050183

Putirka, K. D. (2008). Thermometers and barometers for volcanic systems. *Rev. mineralogy Geochem.* 69 (1), 61–120. doi:10.2138/rmg.2008.69.3

PVMBG (2014). Data dasar gunung api Krakatau. Available at: https://vsi.esdm.go.id/index.php/gunungapi/data-dasar-gunungapi/509-g-krakatau (Accessed 17 Mei 2022).

PVMBG (2022). *Anak Krakatau tanggal 24 april 2022 menjadi level III (siaga)*. Available at: https://magma.esdm.go.id/v1/press-release/214?signature=a181f14600c6e6b59d977187626ea75733b60b653d270f8a44c8a8a7c4ee1712 (Accessed 17 Mei 2022).Press release peningkatan tingkat aktivitas G.

Sakra, S. M., Bamousa, A. O., Gougazeha, M. H., and Zamana, H. (2020). Petromagnetic investigations of the volcanic rocks in southern part of Al-madinah, Saudi arabia: differentiation of different lava types. *J. Taibah Univ. Sci.* 14 (1), 1009–1022. doi:10.1080/16583655.2020.1796477

Self, S. (1992). Krakatau revisited: the course of events and interpretation of the 1883 eruption. *GeoJ* 28 (2), 109–121. doi:10.1007/BF00177223

Self, S., and Rampino, M. R. (1981). The 1883 eruption of Krakatau. *Nature* 294, 699–704. doi:10.1038/294699a0

Silva, P. F., Henry, B., Marques, F. O., Font, E., Mateus, A., Vegas, R., et al. (2008). Magma flow, exsolution processes and rock metasomatism in the Great Messejana-Plasencia dyke (Iberian Peninsula). *Geophys. J. Int.* 175, 806–824. doi:10.1111/j.1365-246X.2008.03920.x

Simkin, T., and Fiske, R. S. (1983). *Krakatau 1883 -eruption and its effects*, 464. Washington, D. C: Smithson Institution. doi:10.1002/esp.3290100118

Siregar, N. D., Rifai, H., Syafriani, S., Fauzi, A., and Mufit, F. (2022). Magnetic susceptibility of volcanic rocks from Pahae Julu region, North sumatera Province. *J. Phys. Appl.* 4, 42–46. doi:10.14710/jpa.v4i2.13597

Stehn, C. E. (1929). The geology and volcanism of the Krakatau group. in *Guidebook for 4th pacific science congress*, 1–55. doi:10.1007/BF00177223

Stormer, J. C. (1983). The effects of recalculation on estimates of temperature and oxygen fugacity from analyses of multicomponent iron-titanium oxides. *Am. Min.* 68, 586–594.

Sutawidjaja, I. (2006). Pertumbuhan gunung api Anak Krakatau setelah letusan katastrofis 1883. *J. Geol. Indones.* 1, 143–153. doi:10.17014/ijog.vol1no3.20063

Tan, W., Liu, P., He, H., Wang, C. Y., and Liang, X. (2016). Mineralogy and origin of exsolution in Ti-rich magnetite from different magmatic FeTi oxide-bearing intrusions. *Can. Mineral.* 54 (3), 539–553. doi:10.3749/canmin.1400069

Tugrul, A., and Gurpinar, O. (1997). The effect of chemical weathering on the engineering properties of eocene basalts in northeastern Turkey. *Environ. Eng. Geosci.* III, 225–234. doi:10.2113/gseegeosci.III.2.225

Unganai, D. A. B., Imai, A., Takahashi, R., Jamal, D. L., Agangi, A., Hoshide, T., et al. (2022). Genesis of magmatic ilmenite ores associated with the Mazua ultramafic intrusion, NE Mozambique. *Ore Geol. Rev.* 143, 104760. doi:10.1016/j.oregeorev.2022.104760

Vidal, C. M., Komorowski, J. C., Métrich, N., Pratomo, I., Kartadinata, N., Prambada, O., et al. (2015). Dynamics of the major plinian eruption of Samalas in 1257 AD (Lombok, Indonesia). *Bull. Volcanol.* 77, 73–24. doi:10.1007/s00445-015-0960-9

Walter, T. R., Haghshenas Haghighi, M., Schneider, F. M., Coppola, D., Motagh, M., Saul, J., et al. (2019). Complex hazard cascade culminating in the Anak Krakatau sector collapse. *Nat. Commun.* 10 (1), 4339. doi:10.1038/s41467-019-12284-5

Westerveld, J. (1952). Quaternary volcanism on Sumatra. *Geol. Soc. Am. Bull.* 63 (6), 561–594. doi:10.1130/0016-7606(1952)63[561:qvos]2.0.co;2

Winchester, S. (2003). *Krakatoa: The day the world exploded, August 27, 1883*. Thorndike Press Available at: https://books.google.co.id/books?id=HReJI5R1yMcC.

Wilson, C. J., Barker, S. J., Charlier, B. L., Myers, M. L., and Hansen, K. F. (2021). A comment on: magma residence and eruption at the taupō volcanic center (taupō volcanic zone, New Zealand)—insights from rhyolite-MELTS geobarometry, diffusion chronometry, and crystal textures, by AS pamukçu et al., contrib mineral petrol 175: 48 (2020). *Contributions Mineralogy Petrology* 176 (10), 79. doi:10.1007/s00410-021-01839-9

Xu, Z.-H., Yang, Z.-F., An, X.-H., Xu, R., and Qi, J.-N. (2022). Relationship between the texture and composition of titanomagnetite in hannuoba alkaline basalt: A new geospeedometer. *Minerals* 12, 1412. doi:10.3390/min12111412

Ye, L., Kanamori, H., Rivera, L., Lay, T., Zhou, Y., Sianipar, D., et al. (2020). The 22 December 2018 tsunami from flank collapse of Anak Krakatau volcano during eruption. *Sci. Adv.* 6, 1377. doi:10.1126/sciadv.aaz1377

Yokoyama, T., Yamada, O., and Nishimura, S. (1983). 14C age of volcanic ash flow at danan island, somma of Krakatau Volcano, Indonesia. *Sci. Eng. Rev. Doshisha Univ.* 24, 78–82.